Two-Dimensional NMR and Photo-CIDNP Studies of the Insulin Monomer: Assignment of Aromatic Resonances with Application to Protein Folding, Structure, and Dynamics†

Michael A. Weiss,*,‡,§ Dzung T. Nguyen,‖ Igor Khait,⊥ Ken Inouye,# Bruce H. Frank,° Michael Beckage,° Erin O'Shea,‖ Steven E. Shoelson,△ Martin Karplus,‖ and Leo J. Neuringer⊥

Department of Biological Chemistry and Molecular Pharmacology, Harvard Medical School, Boston, Massachusetts 02115, Department of Medicine, Massachusetts General Hospital, Boston, Massachusetts 02114, Department of Chemistry, Harvard University, Cambridge, Massachusetts 02138, Francis Bitter National Magnet Laboratory, Massachusetts Institute of Technology, Cambridge, Massachusetts 02139, Shionogi Research Laboratories, Shionogi and Company, Ltd., Fukushima-ku, Osaka 553, Japan, Lilly Research Laboratories, Eli Lilly and Company, Indianapolis, Indiana 46285, and Joslin Diabetes Center and Department of Medicine, Brigham and Women's Hospital, Harvard Medical School, Boston, Massachusetts 02115

Received April 13, 1989; Revised Manuscript Received July 5, 1989

ABSTRACT: The aromatic ^{1}H NMR resonances of the insulin monomer are assigned at 500 MHz by comparative studies of chemically modified and genetically altered variants, including a mutant insulin (PheB25 → Leu) associated with diabetes mellitus. The two histidines, three phenylalanines, and four tyrosines are observed to be in distinct local environments; their assignment provides sensitive markers for studies of tertiary structure, protein dynamics, and protein folding. The environments of the tyrosine residues have also been investigated by photochemically induced dynamic nuclear polarization (photo-CIDNP) and analyzed in relation to packing constraints in the crystal structures of insulin. Dimerization involving specific B-chain interactions is observed with increasing protein concentration and is shown to depend on temperature, pH, and solvent composition. In the monomer large variations are observed in the line widths of amide resonances, suggesting intermediate exchange among conformational substates; such substates may relate to conformational changes observed in different crystal states and proposed to occur in the hormone–receptor complex. Additional evidence for multiple conformations in solution is provided by comparative studies of an insulin analogue containing a peptide bond between residues B29 and A1 (mini-proinsulin). This analogue forms dimers and higher-order oligomers under conditions in which native insulin is monomeric, suggesting that the B29–A1 peptide bond stabilizes a conformational substate favorable for dimerization. Such stabilization is not observed in corresponding studies of native proinsulin, in which a 35-residue connecting peptide joins residues B30 and A1; this extended tether is presumably too flexible to constrain the conformation of the B-chain. The differences between proinsulin and mini-proinsulin suggest a structural mechanism for the observation that the fully reduced B29-A1 analogue folds more efficiently than proinsulin to form the correct pattern of disulfide bonds. These results are discussed in relation to molecular mechanics calculations of insulin based on the available crystal structures.

Insulin is central to the hormonal control of metabolism (Cahill, 1971) and has long provided a model system for protein chemistry and molecular biology. Insulin was the first protein whose sequence was determined (Brown et al., 1955); its crystal structure was an early landmark in biophysics (Adams et al., 1969; Blundell et al., 1971); and its pattern of biosynthesis describes a general motif in eukaryotic cell biology (Steiner et al., 1967). The insulin fold is highly conserved, defining a family of insulin-like regulatory proteins (Blundell & Humbel, 1980). Interest in structure–function relationships has recently been stimulated by the cloning of the insulin receptor (Ebina et al., 1985; Ullrich et al., 1985) and by the discovery of mutant insulins associated with diabetes mellitus (Tager et al., 1979; Tager et al., 1980; Shoelson et al., 1983a, 1983b; Haneda et al., 1984).

Insulin is composed of two polypeptide chains, the A-chain (21 residues) and the B-chain (30 residues) linked by two disulfide bonds. Both chains contribute to the molecular surface involved in receptor binding (Pullen et al., 1976). Of particular interest is the C-terminal region of the B-chain (B23–B26). This region is highly conserved and appears to play an important role in insulin action (Pullen et al., 1976; De Meyts et al., 1978). Mutations or chemical modification in this region can reduce or enhance receptor affinity (Inouye et al., 1981; Nakagawa & Tager, 1986, 1987; Mirmira & Tager, 1989). It has been proposed that flexibility in the C-terminal region of the B-chain plays a functional role (Dodson et al., 1979); such flexibility has been modeled by molecular dynamics simulations (Kruger et al., 1987). Crystallographic studies of insulin in different crystal forms have shown overall differences in subunit structure that are in accord with the presence of conformational flexibility (Chothia et al., 1983). The differences appear to result from crystal packing interactions and are propagated nonlocally by

† This work was supported in part by an NIH grant to Prof. Martin Karplus. M.A.W. and S.E.S. were supported by Research Development awards from the American Diabetes Association.

* Address correspondence to this author at the Department of Biological Chemistry and Molecular Pharmacology, Harvard Medical School.

‡ Department of Biological Chemistry and Molecular Pharmacology, Harvard Medical School.

§ Massachusetts General Hospital.

‖ Harvard University.

⊥ Massachusetts Institute of Technology.

Shionogi and Co., Ltd.

° Eli Lilly and Co.

△ Joslin Diabetes Center and Department of Medicine, Brigham and Women's Hospital, Harvard Medical School.

0006-2960/89/0428-9855$01.50/0

the displacement of elements of secondary structure. Such displacements, which require adjustment in multiple side-chain configurations, provide a model for the transmission of conformational change in proteins.

Despite extensive crystallographic and biochemical studies, little is known about the structure and dynamics of insulin in solution. Although the zinc-free monomer is the physiologically active form of the hormone (Cahill, 1971), self-association (dimers, hexamers, and higher-order oligomers) occurs in native insulin at the concentrations required for nuclear magnetic resonance. This had limited detailed NMR analysis in the past (Kowalsky, 1962; Bradbury & Wilairat, 1967; Paselk & Levy, 1974; Bradbury & Brown, 1977; Williamson & Williams, 1979; Bradbury et al., 1981). Tyrosine accessibility has been investigated under a variety of conditions by chemically induced dynamic nuclear polarization (Muszkat et al., 1984). Well-resolved one-dimensional NMR spectra have been obtained at pH 10–12 with partial assignment of the tyrosine resonances by nitration (Bradbury & Ramesh, 1985). However, under such conditions insulin is unstable, precluding the long acquisition times required for 2D NMR study, and there is a significant perturbation in the circular dichroism spectrum of insulin under basic (but not acidic) conditions (Goldman & Carpenter, 1974). The histidine resonances have been assigned in the oligomeric state at neutral pH by comparative study of species variants (Bradbury et al., 1981) and in the dimer under acidic conditions (Cheshnovsky et al., 1983). A study of metal binding to the insulin hexamer has recently been described (Palmieri et al., 1988).

The results of our investigations are presented in four parts. In part I we characterize conditions under which the zinc-free insulin monomer may be studied in solution by two-dimensional NMR methods at 500 MHz. UV difference spectroscopy, circular dichroism (CD),[1] and photochemical NMR (CIDNP) techniques are used to demonstrate that insulin is monomeric at the concentration and conditions used and that native-like structure is retained. Overall characteristics of the ^{1}H NMR spectrum are described in part II. These observations suggest that the insulin monomer exists as an equilibrium distribution of conformational substates; exchange among substates occurs on the millisecond time scale and leads to broadening of a portion of the resonances. In part III, two-dimensional NMR and photo-CIDNP techniques are used to study local and overall aspects of insulin structure and dynamics in solution. The aromatic resonances are assigned as site-specific probes by a combination of mutagenesis and chemical modification and are monitored as a function of protein concentration, temperature, pH, and solvent composition. Corresponding resonances are observed in the spectrum of human proinsulin and in an insulin analogue containing a peptide bond between residues B29 and A1 (mini-proinsulin). In part IV these features are analyzed by comparison with the X-ray structures of insulin (Blundell et al., 1971). Rigid rotation maps (Gelin & Karplus, 1975) of the aromatic residues are calculated with empirical energy functions and used to complement the NMR analysis of their mobility.

Materials and Methods

Biosynthetic human insulin was provided as zinc crystals by Eli Lilly and Co. (Indianapolis, IN). Zinc was removed by gel filtration (Sephadex G-25) in 1% acetic acid. The solution was lyophilized and redissolved in NMR buffer (below); the protein concentration was determined by UV absorbance at 278 nm, with the assumption that a 1 mg/mL solution has an absorbance of 1.05/cm (Frank & Veros, 1968). Biosynthetic human proinsulin was provided by Eli Lilly and Co. and used without further purification; its concentration was determined by UV absorbance at 278 nm, assuming that a 1 mg/mL solution has an absorbance of 0.66/cm. NMR buffer consists of 20% CD_3COOD/80% D_2O (pD 3.0, direct meter reading). The pD was adjusted with aliquots of 20% CD_3COOD/80% D_2O containing 1 M NaOD or 0.5 M ammonium bicarbonate.

Preparation of Insulin Analogues. LeuB24 and LeuB25 variant insulins were prepared by enzymatic condensation of des-octapeptide-insulin [des-(B23–B30)] with an appropriate octapeptide as described by Inouye et al. (1981). Des-pentapeptide-insulin (DPI) was prepared by partial proteolysis with pepsin as described (Danho et al., 1975). Monoiodinated insulin derivatives were prepared under limiting iodination conditions followed by preparative HPLC purification of the unreacted and singly reacted products as described (Frank et al., 1983). Single-chain B29-A1 insulin (mini-proinsulin) was kindly provided J. Markussen (Novo Pharmaceuticals, Denmark).

NMR. Spectra were recorded at 500 MHz at 37 °C at the Francis Bitter National Magnet Laboratory. Two-dimensional experiments were performed by the pure-phase method of States et al. (1982). A total of 1024 points were sampled in t_2; 256 t_1 values were obtained, and the data matrix was zero-filled to 1K × 1K. HOHAHA, COSY, and NOESY spectra were processed with a convolution difference with trapezoidal and shifted-Gaussian apodization. Spectra were obtained in H_2O by solvent presaturation or by selective excitation by use of the binomial method (Hore, 1983). Data were also collected at 500 MHz at the Laboratory of Chemical Physics (National Institutes of Health) and at Varian, Inc. (Palo Alto, CA). 600 MHz data were collected at the NMR Facility at the University of Wisconsin (Madison).

Photo-CIDNP. Experiments were performed with riboflavin (0.4 mM). Solutions were prepared immediately before use from a saturated stock solution of riboflavin in NMR buffer. A 500-MHz probe was constructed at the Francis Bitter National Magnet Laboratory to permit laser irradiation of the sample under computer control. The probe included an off-center quartz light quide and 45° front-surface dielectric reflector, permitting through-coil irradiation of the NMR tube from the side. The light source was an Innova-6 continuous argon laser at 488 nm (Coherent, Inc., Palo Alto, CA). Light-minus-dark difference spectra were calculated in subsequent data processing. The residual acetate resonance at 2.03 ppm was used as a frequency and intensity standard.

Circular Dichroism and UV Difference Spectra. CD data were obtained at 37, 22, and 13 °C on a Jasco 600 spectrophotometer and with quartz cuvettes having path lengths from 0.02 to 5 cm. UV difference spectra at insulin concentrations from 1 to 20 mg/mL were recorded as described by Rupley et al. (1967).

Rigid Rotation Maps. Calculations were performed with the CHARMM program (Brooks et al., 1983) implemented on the CYBER205 at the John von Neumann National Supercomputer Center (Princeton, NJ). Calculations were based on the two-Zn crystal structure of porcine insulin (Adams et al., 1969; Blundell et al., 1971) and repeated for the two independent monomers in the unit cell. Aliphatic CH groups

[1] Abbreviations: A14-(3-I-Tyr)-insulin, chemically modified insulin containing monoiodinated tyrosine at residue A14; A19-(3-I-Tyr)-insulin, chemically modified insulin containing monoiodinated tyrosine at residue A19; photo-CIDNP, photochemically induced dynamic nuclear polarization; CD, circular dichroism; NOE, nuclear Overhauser enhancement.

were treated as a single element (extended atom model); polar hydrogen coordinates were built from the crystal coordinates and explicitly included (Brunger & Karplus, 1988). Electrostatic interactions were modeled with a distance-dependent dielectric constant. Nonbonded and electrostatic interactions were multiplied by a switching function (Brooks et al., 1983) with a cutoff radius of 10.0 Å. Potential surfaces for ring rotation were generated without minimization (rigid rotation) by the method of Gelin and Karplus (1975). The energy was evaluated as a function of side-chain configuration (χ_1 and χ_2) in 10° intervals. The protein structure was not minimized prior to the calculations.

Aggregation State. Protein self-association was monitored by the concentration dependence of (i) near-UV absorption (Rupley et al., 1967) and circular dichroism (Strickland & Mercola, 1976) spectra, whose features are sensitive to ordering of aromatic rings in the dimer interface; (ii) concentration-dependent changes in the NMR spectrum, which reflect exchange between monomeric, dimeric, and oligomeric species; and (iii) the pattern of photo-CIDNP NMR enhancements, which provide a measure of tyrosine solvent accessibility (Muszkat et al., 1984).

Results

Our results are presented in four parts. In part I conditions are determined in which insulin is monomeric at the millimolar protein concentrations required for NMR study. In part II the overall features of the NMR spectrum are described, and individual aromatic resonances are assigned by a combination of mutagenesis and chemical modification. In part III these assignments are used to characterize features of local structure and dynamics. Photo-CIDNP enhancements are observed to be sensitive to tertiary and quaternary structure, indicating differences in tyrosine environments. The aromatic resonances provide site-specific probes for protein self-association. Specific conformational constraints imposed in the dimer are inferred from a comparative study of an insulin analogue containing a peptide bond between residues LysB29 and GlyA1 (miniproinsulin). In part IV the NMR results are analyzed in relation to rigid rotation maps of the aromatic rings calculated from the crystal structures of insulin.

(I) Characterization of Conditions

Zinc-free insulin exists in solution as an equilibrium mixture of monomers, dimers, tetramers, hexamers, and higher-order oligomers. This equilibrium is a complex function of pH, temperature, ionic strength, and solvent composition (Jeffrey & Coates, 1966a,b). At pH 2–3 in aqueous solution insulin is primarily dimeric (K_d = 10^{-5} M), with higher-order oligomers making a significant contribution at protein concentrations greater than 0.2 mM. NMR resonances obtained under such conditions are broad, reflecting higher-order aggregation and intermediate exchange among oligomeric species (data not shown).

To define conditions suitable for NMR study of the insulin monomer, we have used a combination of biophysical methods to determine the monomer concentration as a function of the percent acetic acid in the solution: (i) circular dichroism and near-ultraviolet absorption spectroscopy, (ii) NMR resonance line widths, and (iii) photo-CIDNP techniques. CD and ultraviolet absorption spectra are sensitive in the near UV (250–300 nm) to the ordering of tyrosine rings and have been used to monitor formation of the dimer interface in insulin (Rupley et al., 1967; Strickland & Mercola, 1976). NMR spectra are sensitive to protein aggregation, since longer rotational correlation times lead to line broadening. In addition,

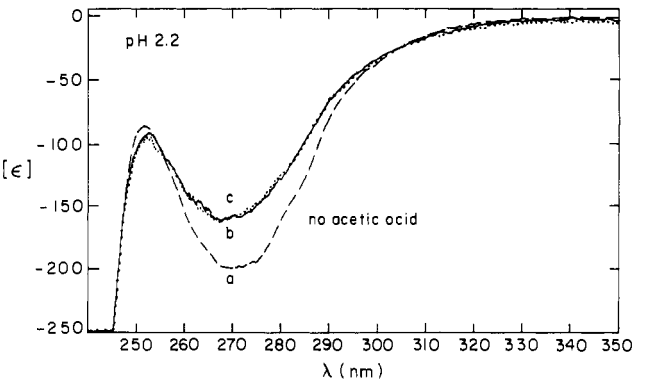

FIGURE 1: Near-UV circular dichroism spectra of zinc-free human insulin are shown at pH 2.2 and 37 °C under the following conditions: (a) 2.5 mM protein concentration in the absence of acetic acid; (b) 2.5 mM protein concentration in 20% acetic acid; (c) 0.1 mM protein concentration in 20% acetic acid.

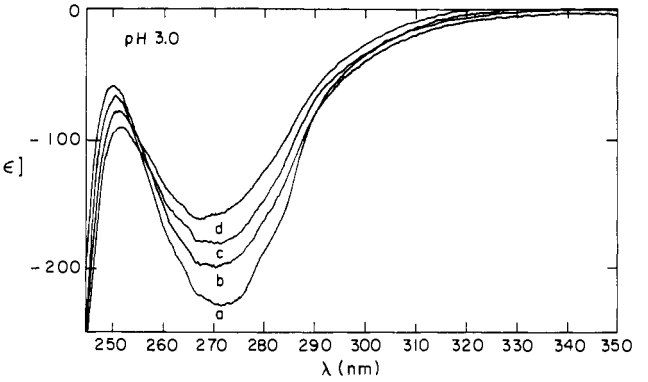

FIGURE 2: Near-UV circular dichroism spectra of zinc-free human insulin are shown in 20% acetic acid–sodium acetate under the following conditions: (a) 1.7 mM protein concentration and 13 °C; (b) 0.17 mM protein concentration and 13 °C; (c) 1.7 mM protein concentration and 37 °C; (d) 0.17 mM protein concentration and 37 °C.

equilibria among oligomeric states can lead to line broadening in the intermediate-exchange regime. Photo-CIDNP NMR enhancements provide a measure of the accessibility of tyrosine residues to collision with a triplet-state probe. Because tyrosine residues are involved in dimerization in the crystal (Blundell et al., 1971) and presumably also in solution, the photo-CIDNP spectrum has been found to vary with aggregation state (Muszkat et al., 1984). These experiments, which also provide controls for the retention of structure under the conditions of the study, are described in turn.

(i) Circular Dichroism and UV Difference Spectroscopy. As the concentration of acetic acid is increased, perturbations are observed in the near-UV circular dichroism spectra (Figures 1 and 2); they are consistent with dissociation of the dimer (Wood et al., 1975; Horuk et al., 1980). In the CD spectrum, for example, dissociation of the dimer leads to attenuation of the negative ellipticity near 273 nm and a shift in the spectral minimum to shorter wavelengths. Corresponding changes are observed in molar UV absorbance (Rupley et al., 1967). These perturbations may be used to determine the fraction of dimers present in the solutions used for NMR studies.

Near-UV CD spectra of zinc-free insulin are shown in Figure 1 at pH 2.2 and 37 °C in the absence of acetic acid (spectrum a) and in 20% acetic acid (spectra b and c). The features observed in spectrum a are characteristic of the insulin dimer and have been attributed to ordering of the B-chain tyrosines (Wood et al., 1975). The observed features and

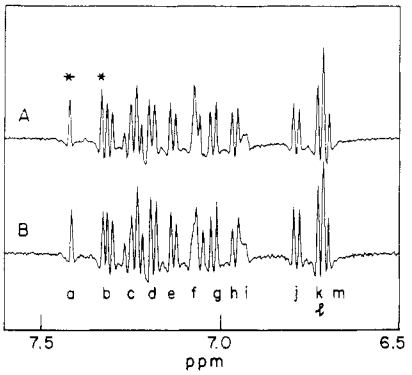

FIGURE 3: Aromatic region of the ^1H NMR spectrum of human insulin in 20% CD_3COOD–80% D_2O (pD 2.2) at 37 °C at 2.4 mM protein concentration (panel A) and 0.2 mM protein concentration (panel B). No significant changes in the NMR spectrum are observed in this concentration range under these conditions. The C_4H resonances of HisB10 (downfield) and HisB5 (upfield) are indicated by asterisks in panel A. Letters refer to assignments given in Table I. The small shift observed in resonance i is due to a 0.04 difference in pD (direct meter reading).

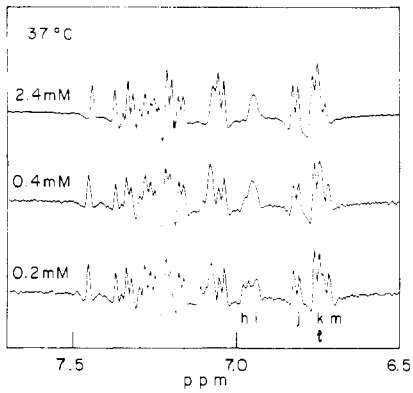

FIGURE 4: Aromatic region of the ^1H NMR spectrum of human insulin in 20% acetic acid–sodium acetate (pD 3.0) at 37 °C at 0.2 mM protein concentration (lower panel), 0.4 mM protein concentration (middle panel), and 2.4 mM protein concentration (upper panel). Significant concentration-dependent features in resonances assigned to TyrB26 (labeled h and m) and PheB24 (labeled i) are observed under these conditions.

magnitude in 20% acetic acid are characteristic of the insulin monomer. No perturbations are observed between insulin concentrations of 0.1 (spectrum c) and 2.5 mM (spectrum b), indicating that the protein remains monomeric under these conditions. Corresponding data at pH 3.0 are shown in Figure 2 under the following conditions: (spectrum a) 1.7 mM protein concentration and 13 °C; (spectrum b) 0.17 mM protein concentration and 13 °C; (spectrum c) 1.7 mM protein concentration and 37 °C; (spectrum d) 0.17 mM protein concentration and 37 °C. At this pH the spectra exhibit concentration-dependent features characteristic of a monomer–dimer transition; significantly more dimerization is observed at 13 °C (spectra a and b) than at 37 °C (spectra c and d).

Concentration-dependent changes in molar UV absorbance are also observed under these conditions (data not shown). The fraction of dimer in solution under these conditions may be estimated, assuming that the difference in molar UV absorbance at 287 nm between the monomer and dimer states is 415–720/cm (Rupley et al., 1967). Thus, a 0.5 mM insulin solution in 20% acetic acid has <2% dimer at 37 °C. In 20% acetic acid–sodium acetate (pH 3.0), a 0.5 mM solution contains 2–5% dimer at 37 °C; such a solution contains 20–40% dimer at 13 °C. That dimerization occurs with increasing protein concentration or decreasing temperature in 20% acetic acid (pH 3) indicates that insulin retains the ability to form quaternary structure under the conditions used for NMR study. UV and CD spectra are not particularly sensitive to the formation of higher-order oligomers under these conditions.

(*ii*) *NMR Characterization of Conditions.* The NMR spectrum of insulin exhibits changes with solvent composition, pH, and temperature which are consistent with those expected from the UV and CD results. As the concentration of acetic acid is increased, the resonances become sharper, and spin systems broadened by intermediate exchange between monomer and dimer (B16, B24, B25, B25; see part II) become better defined. In 20% acetic acid–sodium acetate the spectrum is well-resolved; the dispersion of chemical shifts, which is essentially unaffected by the percentage of acetic acid, is consistent with the retention of folded structure. At pD 2.2 and 37 °C no perturbations are seen with increasing protein concentration in the range 0.2–2.4 mM (Figure 3), consistent with the optical data. At pD 3.0 and 37 °C concentration-dependent changes are observed at these protein concentrations (Figure 4). These changes are consistent with the optical data. NMR resonances exhibiting concentration-dependent perturbations (labeled h, i, and m in Figure 4) are assigned below to the B-chain interface and are more marked at lower temperatures (part III).

(*iii*) *Photo-CIDNP Studies.* Three tyrosine enhancements are observed at 37 °C in 20% acetic acid, assigned below to A14, B16, and B26 (Figure 15; see part III). Since TyrB16 and TyrB26 are known to participate in dimerization (Blundell et al., 1971), this pattern of photo-CIDNP enhancements provides further evidence for dissociation of the dimer (Muszkat et al., 1984). The results are presented in detail in part III.

(II) Two-Dimensional NMR Assignment

Mammalian insulins usually contain four tyrosines, three phenylalanines, and two histidines (Brown et al., 1955). These residues play distinct roles in insulin structure and function. The positions of selected side chains in one protomer of the two-Zn crystal structure (Adams et al., 1969; Blundell et al., 1971) are shown in Figure 5. PheB1 and TyrA14 are on the surface of the protein, whereas TyrA19 and PheB24 participate in the packing of the hydrophobic core. TyrB16, PheB25, and TyrB26 are on or near the surface of the monomer and are involved in dimerization. Both histidines are on the surface of the monomer and engage in subunit interactions in the crystal. HisB10 participates in zinc coordination, and HisB5 is involved in hexamer–hexamer interactions. PheB25 and HisB5 are observed to be in different configurations in the two crystallographic protomers in the two-Zn structure. The functional importance of residues A19, B24, and B25 has been demonstrated by studies of insulin analogues (Pullen et al., 1976) and of mutations associated with diabetes in man (Haneda et al., 1984).

The aromatic spin systems are well-resolved in the 2D NMR isotropic mixing spectrum (HOHAHA), as shown in Figure 6. The histidine resonances are distinct and have been assigned previously (Bradbury et al., 1981; Cheshnovsky et al., 1983). The tyrosine and phenylalanine spin systems are readily distinguished and exhibit equivalent ortho and meta resonances, respectively. A partial assignment of their one-dimensional resonances at pH 10–12 has been reported (Bradbury & Ramesh, 1985). The three phenylalanine systems are selectively visualized in the three-quantum filtered COSY spectrum (data not shown). The individual assignments obtained in this study are based on the comparative 2D NMR

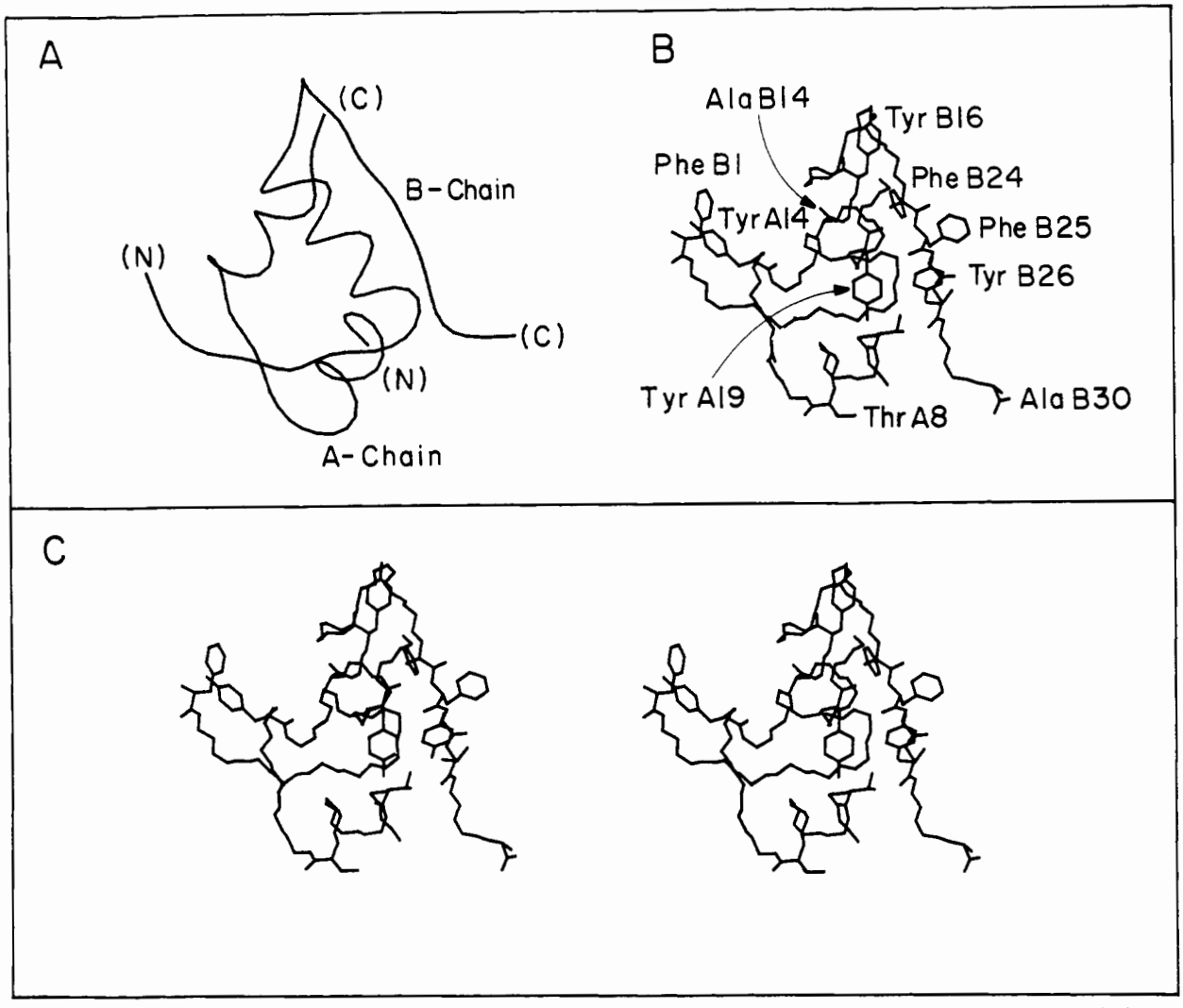

FIGURE 5: (A) Ribbon representation of monomer II in the two-Zn crystal structure of porcine insulin (Blundell et al., 1971) showing the A-chain and B-chain. (B and C) Selected aromatic residues of insulin (PheB1, PheB24, PheB25, TyrA14, TyrA19, TyrB16, and TyrB26) are shown in an α-carbon representation. PheB24 and TyrA19 interact with the hydrophobic core of the hormone. PheB25 is external in molecule II but projects inward toward TyrA19 in molecule I, as shown in Figure 14. TyrB26 is partially exposed in the C-terminal region of the B-chain but also packs against ValB12. TyrB16 and the histidine residues are on the surface of the monomer.

analysis of six insulin species: (i) native human insulin; (ii) PheB24 → Leu mutant insulin; (iii) PheB25 → Leu mutant insulin; (iv) A14-(3-I-Tyr)-insulin derivative; (v) A19-(3-I-Tyr)-insulin derivative; (vi) des-pentapeptide-insulin (DPI; lacking residues B26–B30). The sequences and amino acid compositions of the mutant and modified insulins have been previously characterized (Inouye et al., 1982; Frank et al., 1983).

(*i*) *Sequence-Specific Assignment.* Systematic assignment of protein NMR resonances may be accomplished in certain proteins by the sequential analysis of amide–H_α connectivities (Wuthrich et al., 1983). The amide resonances of the insulin monomer, however, exhibit a large variation in line width, as shown in Figure 7. Many of the amide resonances are quite broad (30–40 Hz); their crosspeaks are not observed in two-dimensional spectra (data not shown). Such variation is more extensive at 600 MHz than at 500 MHz, suggesting an exchange process (data not shown). However, the observed broadening is not due to solvent exchange (i.e., replacement of an amide proton by a solvent proton with kinetics "intermediate" on the NMR time scale), since selective excitation (panel B) and solvent presaturation (panel A) yield similar spectra. If solvent exchange were the primary mechanism of resonance broadening, then replacement of an unsaturated amide proton by a saturated solvent proton would be expected to attenuate the amide resonance involved. This is not observed.

A similar (although less marked) pattern of broadening is observed among the nonexchangeable proton resonances (data not shown). We attribute differential broadening to exchange among conformational substates of the protein. Indeed, less extensive line broadening is observed in the spectrum of a partial proteolytic fragment, des-pentapeptide-insulin (DPI; section iii); presumably, more rapid motions in the fragment lead to more complete averaging of chemical shifts on the NMR time scale (data not shown). For this reason sequential assignment techniques are difficult to apply to native insulin under these conditions, and alternative methods of resonance assignment are required. Comparative studies of chemically modified and genetically altered insulins are used in the present case. Analysis of the observable "fingerprint" region using isotopically labeled amino acids is in progress and will be described elsewhere.

(*ii*) *Assignment of the Phenylalanine Spin Systems by Mutagenesis.* PheB24 and PheB25 are highly conserved and are proposed to interact directly with the insulin receptor (Pullen et al., 1976). Mutations at these positions (PheB24 → Ser and PheB25 → Leu) have been identified in patients with diabetes mellitus (Tager et al., 1979, 1980; Shoelson et al., 1983a,b; Haneda et al., 1984). Their NMR resonances

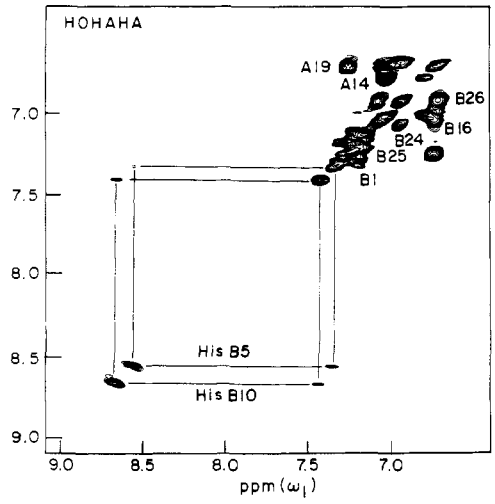

FIGURE 6: Two-dimensional HOHAHA spectrum of 1 mM human insulin in 20% acetic acid–sodium acetate (pD 3.0) at 37 °C. The experiment was performed by the method of Davis and Bax (1985). The mixing time is 30 ms. The two histidine, three phenylalanine, and four tyrosine spin systems are well-resolved. Crosspeaks involving the para resonance of PheB24 are not observed. The crosspeak between C_2H and C_4H resonances of HisB5 is less intense than that of HisB10 due to more rapid $T_{1\rho}$ relaxation during the spin-lock period.

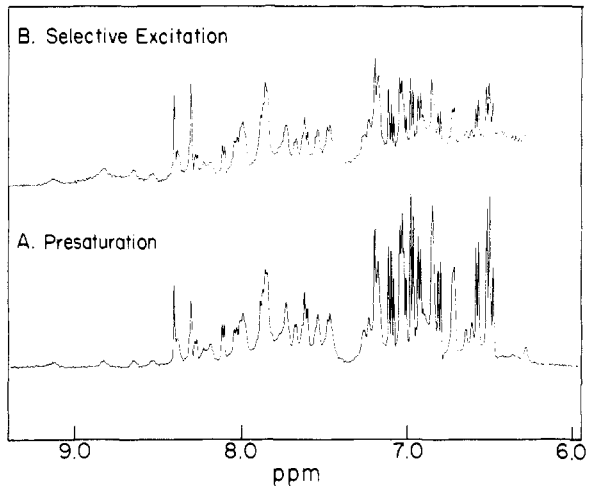

FIGURE 7: A large variation of line widths is observed among the amide resonances in the one-dimensional ^1H NMR spectra of monomeric human insulin in 20% CD_3COOH–80% H_2O at 37 °C. A similar pattern is observed following presaturation of the solvent resonance (panel A) and following selective excitation by a 1–1 selective binomial excitation (panel B). The attenuation of resonances in the upfield portion of spectrum B (6–7 ppm) is due to the characteristic excitation profile of the 1–1 pulse scheme.

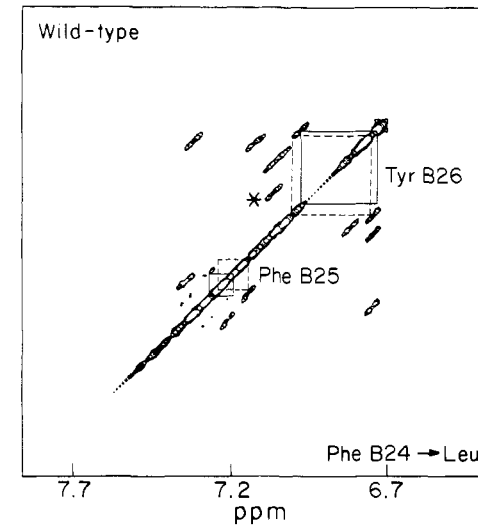

FIGURE 8: Comparison of the aromatic regions of the 2D COSY spectra of native human insulin (upper left) and of the PheB24 → Leu mutant insulin (lower right) at 37 °C in 20% acetic acid–sodium acetate (pD 3.0). The most upfield of the phenylalanine spin systems is absent in the spectrum of the mutant protein, assigning these resonances to PheB24 in the spectrum of the native protein (asterisk). The B25 and B26 spin systems are shown as solid lines in the spectrum of native insulin and as dashed lines in the spectrum of the mutant insulin. In this format perturbations are observed as asymmetries in crosspeak position. The protein concentration was 0.5 mM. Only positive contours are shown.

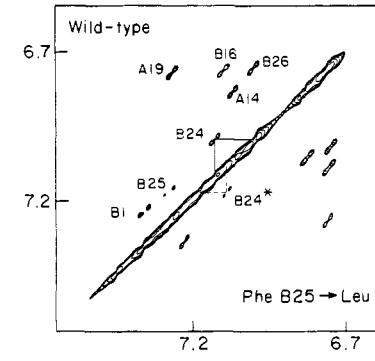

FIGURE 9: Comparison of the aromatic regions of the 2D COSY spectra of native human insulin (upper left) and of the PheB25 → Leu mutant insulin (lower right) at 45 °C in 20% acetic acid–sodium acetate (pD 3.0). One phenylalanine spin system is absent in the spectrum of the mutant protein, assigning these resonances to PheB25 in the spectrum of the native protein (Table I). The resonances of PheB24 are shifted downfield in the spectrum of the mutant protein (asterisk). The native spectrum differs from that shown in Figure 8 due to a difference in temperature; conditions are otherwise as described in Figure 8.

are assigned by comparison of wild-type and mutant insulins containing leucine substitutions. Leucine was chosen to correspond to the diabetes-associated mutation at B25.

The 2D-COSY spectra of LeuB24 and LeuB25 insulin are compared with the native insulin spectrum in Figures 8 and 9, respectively. One phenylalanine spin system is absent in each of these spectra, as expected from their amino acid compositions. PheB24 is assigned as the most upfield of the phenylalanine spin systems. The resonances of PheB25 are intermediate between PheB24 and those of the remaining phenylalanine spin system, which is assigned to PheB1 by elimination (see Table I); the chemical shift of PheB1 is near that of free phenylalanine. Additional perturbations are observed in the spectra of the mutant insulins, as is evident in Figures 8 and 9. These may reflect structural or dynamic perturbations and/or magnetic effects resulting from the replacement of an aromatic residue (phenylalanine) by a nonaromatic residue (leucine). Detailed characterization of these mutant insulins will be given elsewhere.

In native insulin the resonances of PheB24 are broadened; the para resonance is not observed and may overlap the ortho resonance. The broadening of the B24 resonance suggests that it is in intermediate exchange among related ring configurations; such exchange may involve constrained ring rotation about χ_2 or more extended motions including χ_1 and χ_2 (e.g., ring sliding). The apparent absence of a sharp para resonance suggests the latter mechanism is involved, since it would not be broadened by ring rotation. In the crystal state electron density for PheB24 is well-defined in a single configuration. However, this configuration is stabilized by aromatic–aromatic interactions with the dimer-related PheB24′ and TyrB26′, which would not be present in the monomer. The functional

Table I: Aromatic Assignments at 30 °C at pD 2.2 (ppm Relative to Acetate, Assumed To Be 2.03 ppm)

		resonance	ppm
A14	ortho	g	7.036
	meta	j	6.806
A19	ortho		7.281
	meta	k, l	6.742
B1	ortho	d	7.202
	meta	b	7.325
	para	c	7.263
B5	H_2[a]	–	8.573
	H_4	b	7.384
B10	H_2[a]	–	8.671
	H_4	a	7.448
B16	ortho	f	7.060
	meta	k, l	6.737
B24	ortho	i	7.070
	meta	f	6.943
	para		*b*
B25	ortho	e	7.168
	meta	c	7.247
	para	d	7.202
B26	ortho	h	7.007
	meta	m	6.752

[a] The C_2H resonances of HisB5 and HisB10 are not shown in Figure 3. [b] The para resonance of PheB24 has not been located in the ^1H NMR spectrum.

importance of alternative configurations is suggested by the enhanced bioactivity of a D-PheB24 analogue (Kobayashi et al., 1982).

The resonances of PheB1 are sharper than those of PheB24 or PheB25. They exhibit few NOEs, indicating that the N-terminus of the B-chain is flexible in solution (data not shown). The resonances of PheB25 are intermediate between B1 and B24 in both chemical shift and line width. Although PheB25 is observed in two configurations in the crystallographic dimer (Peking Insulin Structure Group, 1971; Blundell et al., 1971), there is no evidence for two distinct configurations in solution.

(iii) Assignment of the Tyrosine Spin Systems by Chemical Modification. TyrB26 is assigned by comparison of insulin and a partial proteolytic product, des-pentapeptide-insulin (DPI). This derivative lacks the five C-terminal residues of the B-chain (TyrB26, ThrB27, ProB28, LysB29, and ThrB30). One tyrosine spin system is absent in the spectrum of DPI, which is assigned accordingly to B26 (data not shown). TyrA14 and A19 are assigned by selective monoiodination at the H_3 ring position in singly modified insulin. In one-dimensional spectra this modification results in a downfield shift of H_2, which is a singlet resonance in the absence of H_3 (labeled m in Figures 16 and 17; part III). The aromatic region of the COSY spectrum of the A14 derivative is shown in Figure 10. Modification of A14 selectively alters the A14 spin system; the A14 H_5–H_6 connectivity has half the amplitude of the corresponding $H_{2,6}$–$H_{3,5}$ connectivity in the COSY spectrum of the native protein and exhibits a downfield shift. The other aromatic resonances are observed to be unperturbed, indicating an absence of nonlocal perturbations. The A19 spin system is assigned similarly, as shown in Figure 11. The resonances of B16 are assigned by elimination.

Iodination of A19 results in significant perturbations in the ^1H NMR spectrum, as observed in the COSY spectrum (Figure 11) and in its photo-CIDNP spectrum (part III). Shifts are seen in the crosspeaks of PheB24 and TyrB26. These transmitted perturbations would be anticipated from the crystal structure (Figure 5) and provide a control for the retention of tertiary interactions in solution. The resonances of PheB25 are not perturbed. The A19 derivative appears to

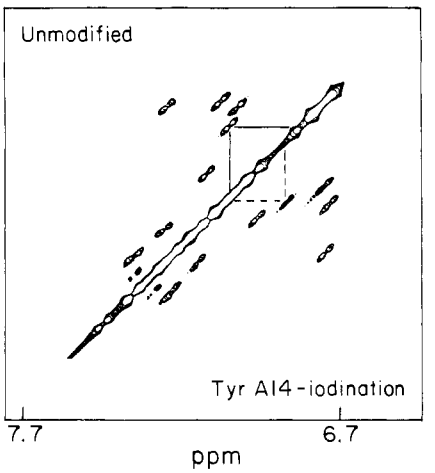

FIGURE 10: Comparison of the aromatic regions of the 2D COSY spectra of native human insulin (upper left) and of A14-(3-I-Tyr)-insulin (lower right) at 37 °C in 20% acetic acid–sodium acetate (pD 3.0). The TyrA14 and 3-I-TyrA14 spin systems are outlined in solid and dashed lines, respectively. The remaining crosspeaks are not significantly perturbed by this modification, which is consistent with the position of TyrA14 in the crystal structure (Figure 5). Conditions were as described in the legend to Figure 8.

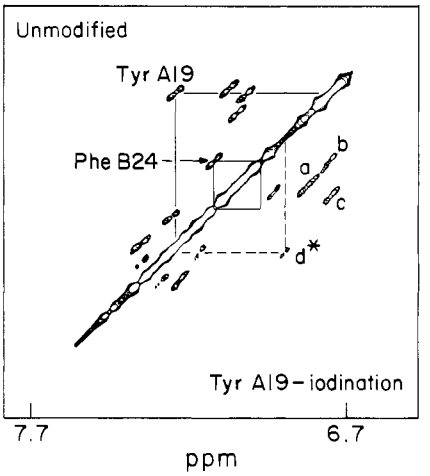

FIGURE 11: Comparison of the aromatic regions of the 2D COSY spectra of native human insulin (upper left) and of A19-(3-I-Tyr)-insulin (lower right) at 37 °C in 20% acetic acid–sodium acetate (pD 3.0). The TyrA19 and 3-I-TyrA19 (crosspeak d*) spin systems are outlined in solid and dashed lines, respectively. Significant perturbations are observed in the resonances of PheB24 and TyrB26 (b). Perturbations are not seen in the crosspeaks of TyrB16 (c) and TyrA14 (a). Conditions were as described in the legend to Figure 8.

dimerize more readily than does native insulin, as indicated by the concentration dependence of the NMR spectrum (data not shown). Corresponding changes are seen in the near-UV region of the CD spectrum (B. Frank, unpublished results). The structural basis for this is not clear, since in the crystal state TyrA19 does not participate in the dimer interface (Blundell et al., 1971).

Of the tyrosine resonances A14 exhibits the narrowest line width and A19 the broadest, as indicated by the intensity of their COSY crosspeaks (Weiss et al., 1984). In the modified protein the A19 H_2 singlet resonance is broader than the corresponding resonance in the spectrum of the A14 derivative. This broadening is similar to that exhibited by PheB24 and can also arise from barriers to ring rotation and/or more extended motions of the tyrosine side chain. The B16 and B26 resonances have line widths intermediate between those of A14 and A19. This pattern of relative line widths corresponds to

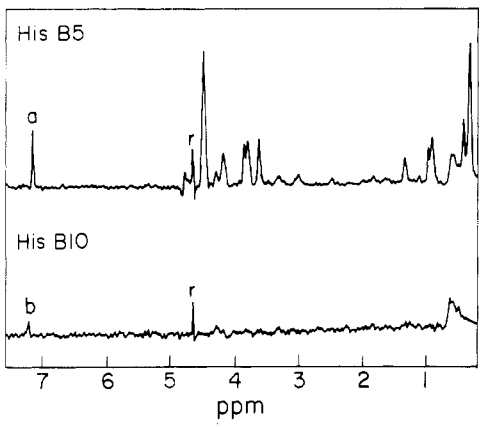

FIGURE 12: Slices through the NOESY spectrum of human insulin in 20% acetic acid at 37 °C. The mixing time was 400 ms. The slice shown in the upper panel contains crosspeaks involving the C_2H resonance of histidine B5; the slice shown in the lower panel contains crosspeaks involving the C_2H resonance of HisB10. In each slice an NOE is seen to the C_4H resonance of the same residue (labeled a in the upper panel and b in the lower panel); their relative intensity reflects local structure and dynamics. The residual HOD resonance is labeled r.

the pattern of photo-CIDNP enhancements (part III). This correspondence is likely to reflect a common structural mechanism: the existence of side-chain interactions which both constrain local motions and limit accessibility to radical-pair formation.

(*iv*) *Histidine Resonances.* The resonances of HisB5 and HisB10 were previously assigned by Bradbury and colleagues by comparative studies of human insulin, hagfish insulin (lacking HisB10), and a HisB5 → Ala insulin analogue (Bradbury et al., 1981; see Table I). The ring resonances of HisB10 also exhibit significantly fewer crosspeaks in the NOESY spectrum than those of HisB5 (Figure 12). In the crystal each of the histidine residues is on the surface of the monomer; however, HisB5 participates in more local interactions (including hydrogen bonding; part III) than HisB10 (Blundell et al., 1971). In solution these interactions evidently permit more efficient dipolar relaxation with neighboring protons, influencing the observed line width and pattern of NOEs. Perturbation of the histidine resonances with self-association and temperature are described in part III(iii).

(III) Structural and Dynamic Features

The aromatic resonances provide site-specific probes for the characterization of (i) structural relationships by nuclear Overhauser enhancements (NOEs), (ii) tyrosine accessibilities by photo-CIDNP methods, (iii) exchange features due to temperature-dependent ring dynamics, (iv) exchange phenomena due to specific protein–protein interactions in solution, and (v) conformational constraints in an insulin analogue containing a cross-link between residues B29 and A1 (miniproinsulin). We discuss each of these in turn.

(*i*) *Structural Relationships.* The aromatic region of the NOESY spectrum, shown in Figure 13, demonstrates that there are no crosspeaks between aromatic residues. This is the case even at longer mixing times (up to 400 ms) when indirect effects are likely to be observable. Of particular interest is the absence of an NOE between PheB25 and TyrA19. In addition, no NOEs are observed in common between α- or β-protons and the ring protons of A19 and B25 (data not shown). In the two-Zn crystal an interaction between these rings is predicted in one protomer (molecule I) but is not predicted in the other protomer. This difference arises from the asymmetry of the insulin dimer that involves a large

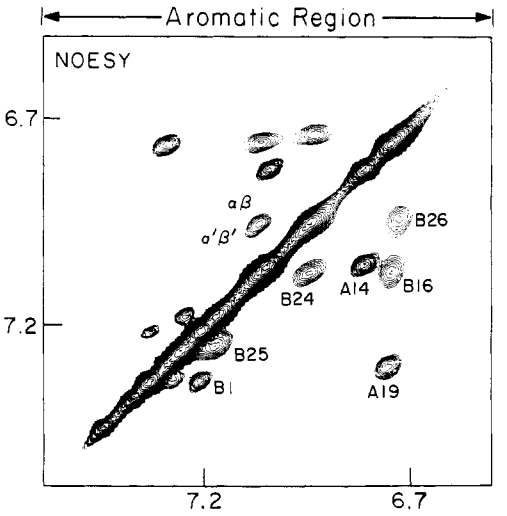

FIGURE 13: Aromatic region of the NOESY spectrum of human insulin under the conditions described in the legend to Figure 14. The assignments shown are given in Table I. The mixing time was 400 ms. Despite the long mixing time, only intraresidue crosspeaks are observed. The PheB24 crosspeak is elongated parallel to the diagonal, indicating exchange between two states, labeled $\alpha\beta$ and $\alpha'\beta'$.

Table II: Interproton Distances (Å) between A19 and B25 in the Two-Zn Crystal[a]

	A19						
B25	H_α	H_{β_1}	H_{β_2}	H_{δ_1}	H_{δ_2}	H_{ϵ_2}	H_{ϵ_2}
H_α							
mol I	6.8	5.6	6.9	6.9	9.1	9.0	10.9
mol II	6.7	5.6	7.3	5.8	7.7	9.3	10.6
H_{β_1}							
mol I	6.3	5.8	7.4	6.4	9.4	8.6	11.0
mol II	5.7	5.2	6.9	**4.3**	5.6	8.4	9.2
H_{β_2}							
mol I	6.3	5.4	7.0	5.3	8.9	7.6	10.2
mol II	**4.2**	**4.1**	5.8	**3.6**	5.4	7.4	8.4
H_{δ_1}							
mol I	5.0	**4.2**	5.0	**3.6**	7.4	5.4	8.4
mol II	5.4	5.7	7.2	5.9	7.9	9.0	10.4
H_{δ_2}							
mol I	**4.5**	**4.8**	6.2	5.7	8.1	8.0	9.9
mol II	7.7	7.3	9.1	6.5	7.6	10.6	11.4
H_{ϵ_1}							
mol I	**4.1**	**4.2**	5.8	**2.4**	6.6	**3.6**	7.2
mol II	7.7	8.2	9.6	8.7	10.0	11.5	12.8
H_{ϵ_2}							
mol I	**2.9**	**4.5**	5.6	4.8	7.1	6.8	8.6
mol II	9.5	9.4	11.2	9.5	9.8	12.8	13.5
H_ζ							
mol I	**2.7**	**4.2**	5.4	**3.1**	6.3	**4.6**	7.2
mol II	9.5	9.8	11.4	9.5	10.9	13.2	14.2

[a] Proton coordinates were extrapolated from the heavy-atom coordinates (Blundell et al., 1971) with the CHARMM program (Brooks et al., 1983). Distances corresponding to nonnegligible NOEs (<5 Å) are shown in boldface.

change in the configuration ($\Delta\chi_1 = 120°$) of PheB25. The interproton distances calculated from these structures are given in Table II; the alternative ring orientations of A19 and B25 are illustrated in Figure 14. The absence of a PheB25–TyrA19 NOE suggests that in solution PheB25 extends outward rather than inward. This is perhaps surprising because in the energy-minimized structure the configuration of PheB25 observed in molecule I appears more stable that the configuration observed in molecule II (Wodak et al., 1984; data not shown). Differences between internal and surface residues are also apparent in the pattern of NOEs involving nonaromatic protons. The predominant aromatic–methyl NOEs, for example, involve PheB24 and TyrA19, reflecting stable packing

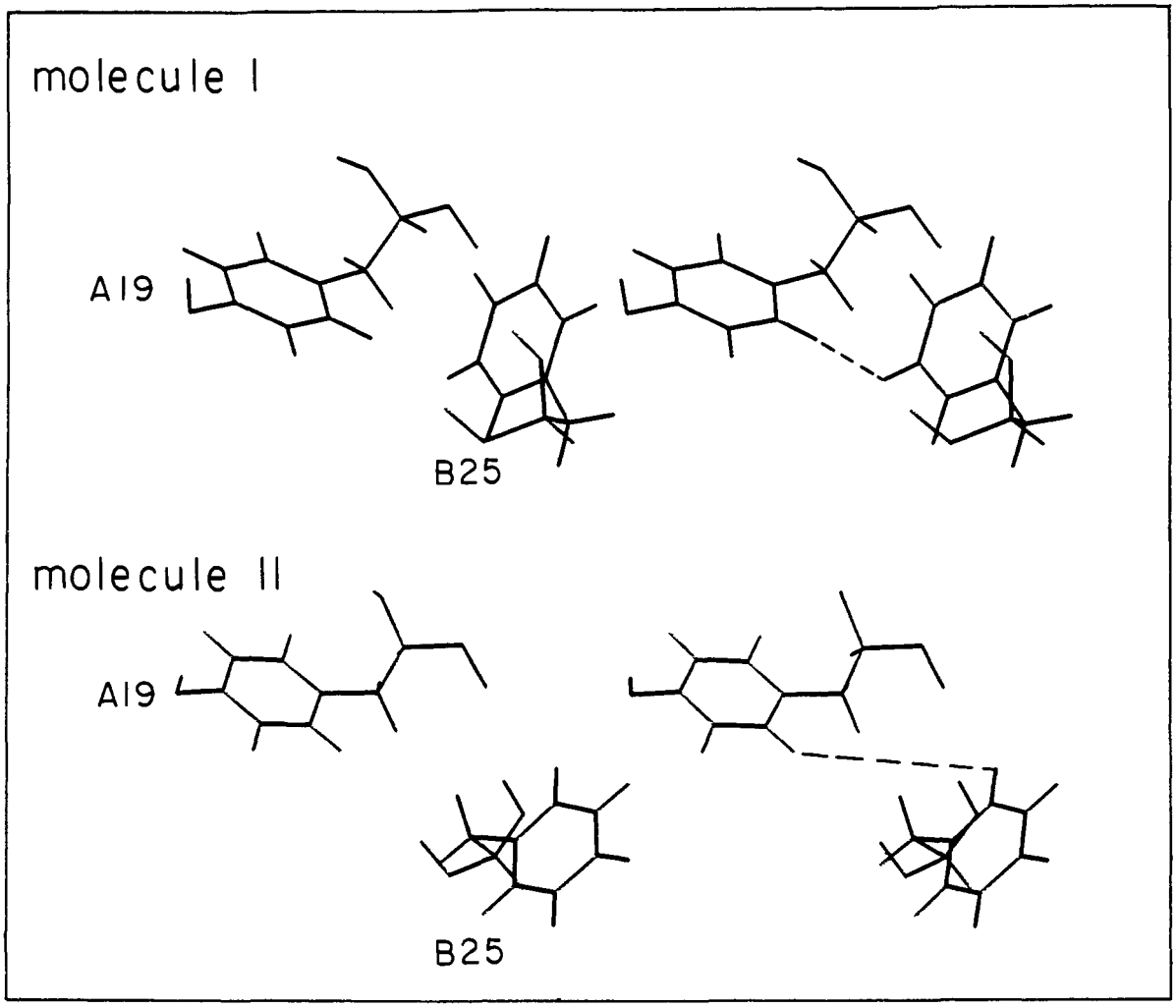

FIGURE 14: Stereo representation of the relative orientation of PheB25 and TyrA19 in molecule I (upper panel) and molecule II (lower panel) in the two-Zn insulin crystal structure (Blundell et al., 1971). The dashed lines indicate the closest distances between ring protons in the two orientations (see Table II).

interactions as between, for example, A19 and IleA2 (data not shown). Such NOEs are not observed for PheB25.

The absence of an NOE between TyrA19 and PheB25 is also consistent with the absence of its perturbation following monoiodination of A19 (see above). However, the interaction between H_{δ_1} of TyrA19 and H_{β_2} of PheB25 predicted for molecule II (Table II) is also not observed. This interaction depends on χ_1 and is nonnegligible for only a narrow range of configurations. If PheB25 were flexible in the monomer, then such an NOE would not be expected from an ensemble of structures due to r^{-6} averaging and attenuation of cross-relaxation by rapid local motions. The flexibility of PheB25 as a surface residue is also suggested by its small secondary shift and line width.

(*ii*) *Tyrosine Accessibility*. The environment of individual tyrosine residues can be investigated by photochemically induced dynamic nuclear polarization (photo-CIDNP). This technique is based on a reversible photochemical reaction of protein side chains (tyrosine and histidine) with a dye excited to the triplet state (Kaptein, 1980; Berliner & Kaptein, 1981). This reaction leads to a transient spin-correlated radical pair involving the reversible transfer of a hydrogen from the tyrosine hydroxyl or histidine imidazole (A) to the photoexcited dye (D):

$$AH + {}^3D \rightarrow \overline{{}^3A\text{-}DH} \rightarrow AH^* + D \qquad (1)$$

The resulting change in the intensity and sign of the nuclear transitions yields a 5–15-fold amplification, which is specific for the group involved in the hydrogen transfer (Muszkat & Gilon, 1978). Because a productive collision is required between the protein residue and the dye, photo-CIDNP may be used to identify individual tyrosine or histidine residues on the surface of a protein. Resonances from histidine are not enhanced under acidic conditions due to protonation of the imidazole ring (Kaptein, 1980; Muszkat et al., 1984).

The insulin monomer exhibits a simple pattern of photo-CIDNP enhancements at 500 MHz (Figure 15). The dark, light, and difference spectra at 37 °C are shown in panels A–C, respectively. Three enhanced signals are observed, corresponding to TyrA14 (resonance a), TyrB26 (resonance d), and a third signal (resonance b); the intensity ratio $a/(b + d)$ is 1:1.8. The meta resonances of TyrB16 and TyrA19 at position b are unresolved at this temperature but are partially resolved at 20 °C (Figure 19). The corresponding difference spectrum at 20 °C indicates that enhancement d is due to TyrB26 (data not shown). The enhancement of TyrB16 (resonance b) is somewhat greater than that of B26. Enhancement of TyrA19 is not observed. This is consistent with its internal position in the crystal structure. The photo-CIDNP results differ from those obtained from studies of iodination rates, as TyrA19 is more readily iodinated than the B-chain tyrosines (Linde & Hansen, 1980). This presumably reflects rate enhancement in the A19 hydrophobic pocket (local catalysis) rather than increased accessibility to reactant.

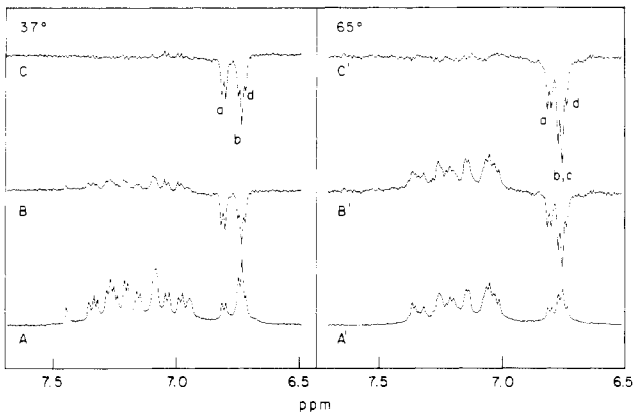

FIGURE 15: Photo-CIDNP studies of human insulin in 20% CD_3C-OOD (pD 1.8) demonstrate differential reactivity of the tyrosine rings to dynamic nuclear polarization. Spectra at 37 and 65 °C are shown in the absence of photoexcitation (panels A and A′) and following photoexcitation (panels B and B′); the resulting difference spectra are shown in panels C and C′. At 37 °C (panels A–C) three enhancements are observed, assigned to TyrA14 (labeled a in the difference spectrum shown in panel C), TyrB16 (labeled b in the difference spectrum), and TyrB26 (labeled d in the difference spectrum). No enhancement is observed from TyrA19. However, at 65 °C (panels A′–C′) integration of the difference spectrum indicates that all four tyrosines (including TyrA19, labeled c) exhibit polarization. The protein concentration was 0.5 mM. The spectra shown in panels A and A′ were processed without weighting functions; those in panels B, B′, C, and C′ were processed with 2-Hz exponential multiplication for sensitivity enhancement.

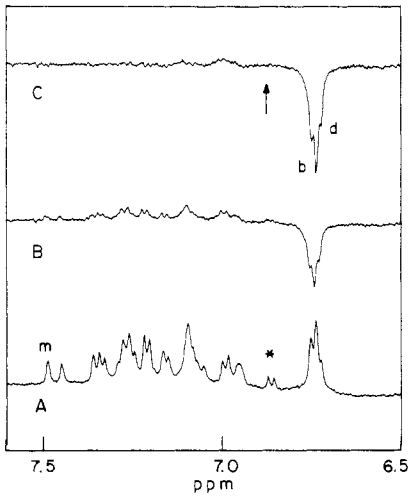

FIGURE 16: Photo-CIDNP studies of A14-(3-I-Tyr)-insulin at 37 °C in 20% CD_3COOD (pD 1.8) demonstrate selective quenching (indicated by an arrow in panel C) of the polarization of TyrA14 in the presence of the iodo substituent. Spectra in the absence of photoexcitation (panel A) and following photoexcitation (panel B) and a difference spectrum (panel C). Two remaining enhancements are observed, assigned to TyrB16 (labeled b in the difference spectrum) and TyrB26 (labeled d in the difference spectrum). As in the native protein, no enhancement is observed from TyrA19. The H_2 singlet resonance from the modified tyrosine ring is labeled m in panel A. The asterisk indicates the H_5 resonance of the modified ring. The protein concentration was 0.5 mM. Spectra were processed as described in the legend to Figure 15.

Assignments in the photo-CIDNP difference spectra are verified through comparative studies of the monoiodotyrosine derivatives. Enhancement is quenched due to the low-lying triplet state accessible to the modified ring. This effect is illustrated in the spectrum of A14-(3-I-Tyr)-insulin (Figure 16). Although resonances b and d are present in the difference spectrum (panel C), no enhancement is observed for the H_5 resonance from TyrA14 (indicated by an asterisk in panel A and by an arrow in panel C). The corresponding data for

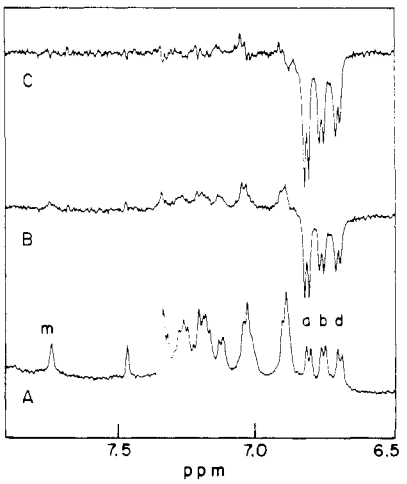

FIGURE 17: Photo-CIDNP studies of A19-(3-I-Tyr)-insulin at 37 °C in 20% CD_3COOD (pD 1.8) are consistent with the absence of polarization from TyrA19. Spectra shown in the absence of photoexcitation (panel A) and following photoexcitation (panel B) and a difference spectrum (panel C). As in the native protein, three enhancements are observed, similarly assigned to TyrA14 (labeled a in panel A), TyrB16 (labeled b), and TyrB26 (labeled d). The H_2 singlet resonance from the modified tyrosine ring is labeled m. The protein concentration was 0.5 mM. Spectra were processed as described in the legend to Figure 15.

A19-(3-I-Tyr)-insulin are shown in Figure 17. Fortuitously, the four tyrosine meta resonances are resolved, and so photo-CIDNP enhancements may be assigned without ambiguity. Enhancements are observed for A14 (resonance a), B16 (resonance b), and B26 (resonance d). The ratio of $a/(b + d)$ is 1:1.5. The decrease in the enhancement of B16 + B26 relative to A14 is likely to represent partial dimerization; the enhancement of the B-chain tyrosines relative to A14 increases with dilution of the A19 derivative. Perturbations in the near-UV region of the CD spectrum of the A19 derivative are also observed and suggest enhanced dimerization (B. Frank, unpublished results). Structural perturbations in the modified protein are also possible and may alter the photo-CIDNP reaction.

The inaccessibility of TyrA19 to photo-CIDNP enhancement provides a marker for tertiary structure and may be used to follow protein unfolding. At higher temperatures (>65 °C), amplitude corresponding to four tyrosine signals is observed, as illustrated in panels A′, B′, and C′ of Figure 15. Thus, there is a progressive increase in the A19 enhancement with increasing temperature. In addition, there is a loss of chemical shift dispersion between 30 and 80 °C, suggesting a progressive equilibrium between folded and unfolded forms. The largest changes in chemical shift are in general observed for those residues whose secondary shift in the folded state is greatest, as expected for denaturation. In the case of insulin these are B24 and A19. These temperature-dependent changes in chemical shifts are summarized in Figure 18. Changes in photo-CIDNP enhancements are also observed with decreasing percentage of acetic acid, as described in section iv.

(*iii*) *Temperature-Dependent Ring Dynamics.* The temperature dependence of the aromatic NMR spectrum from 0 to 45 °C is shown in Figure 19 at pD 1.8 in 20% acetic acid. Insulin remains monomeric over this temperature range, as indicated by corresponding CD and UV difference spectra (see part I). There is an overall broadening of the spectrum with decreasing temperature, consistent with slower molecular tumbling. In addition, features associated with exchange phenomena are observed involving HisB5, TyrA19, PheB24, and TyrB26.

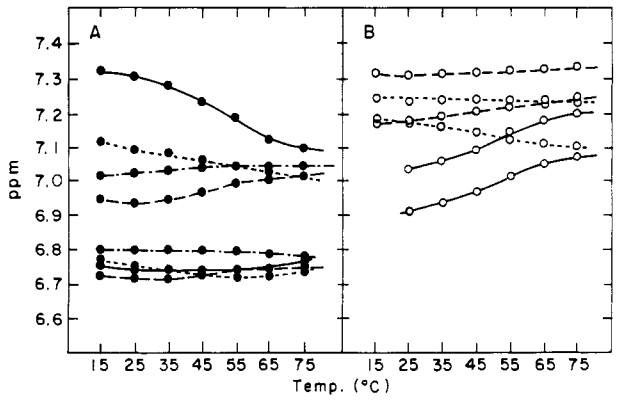

FIGURE 18: Chemical shifts of the aromatic resonances are shown as a function of temperature. The tyrosine resonances are plotted in the left-hand panel (filled-in circles), and the phenylalanine resonances are plotted in the right-hand panel (open circles). The largest changes with increasing temperatures are observed for PheB24 and TyrA19 (solid lines), which exhibit the largest secondary shifts. The B26 resonances are drawn with long dashed lines, the B16 and B25 resonances are drawn with short dashed lines, and A14 resonances are drawn with dot-dashed lines.

HisB5 (resonance b) is observed to broaden as the temperature is lowered, whereas in the absence of self-association HisB10 (resonance a) remains sharp. Such broadening suggests that HisB5 is in exchange between different configurations, and with decreasing temperature, this exchange goes from fast to intermediate on the NMR time scale. In the two-Zn crystal distinct B5 configurations (with different hydrogen-bonding schemes) are observed in the dimer (Blundell et al., 1971). Disproportionate broadening is also observed in the resonances of PheB24 (resonance i) and TyrA19 (resonance l), reflecting packing constraints in their environments. Simple ring rotation cannot be distinguished from more extended motions (e.g., ring sliding) by these data. Broadening is also observed for TyrB26 at 0–5 °C (resonances j and m). The observed changes in line width are greater than that expected for a protein of this size due solely to the temperature dependence of overall rotation, as indicated by NMR studies of other small globular proteins.

(*iv*) *Specific Protein–Protein Interactions.* Dimerization at pD 3 at 37 °C also leads to broadening of resonances assigned to residues in the dimer interface (PheB24, PheB25, TyrB16, TyrB26). These were shown in Figure 4 (part I). With further increases in protein concentration, the resonances of HisB10 also broaden, presumably reflecting dimer–dimer interactions as in the crystal (Blundell et al., 1971). Similar changes are observed as the concentration of acetic acid is reduced (data not shown).

The temperature-dependence of the aromatic NMR spectrum at pD 3 exhibits a more complex pattern of resonance broadening than is observed at pD 1.8, reflecting two distinct mechanisms of intermediate exchange: one due due to motions constrained by tertiary structure (as at pD 1.8) and the other due to self-association. A third mechanism due to packing constraints in the subunit interface is also possible. Because such barriers would only be present when the dimer interface was formed, and because the dimer is present only in an equilibrium mixture of oligomeric species, these mechanisms cannot be presently resolved. TyrA14 and PheB1 are relatively unaffected by these mechanisms (data not shown). In the crystal these residues are on the surface of the protein and are not involved in protein–protein interactions within the hexamer (Blundell et al., 1971).

The pattern of photo-CIDNP enhancements also changes with dimerization. These enhancements are shown in Figure

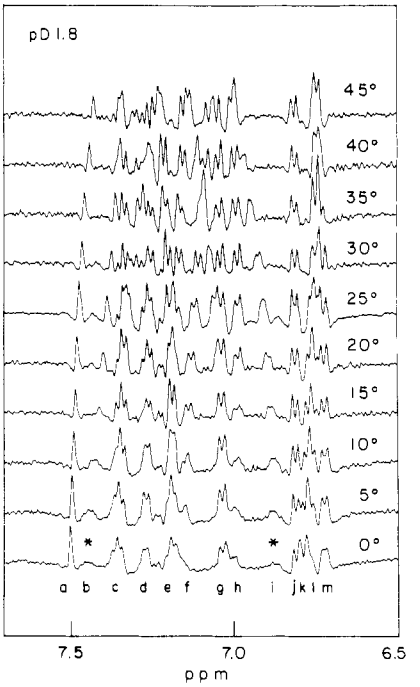

FIGURE 19: Aromatic region of the ^{1}H NMR spectrum of monomeric human insulin is shown as a function of temperature in the range 0–45 °C. The labels in the bottom panel refer to Figure 1. Under these conditions (20% CD_3COOD, pD 1.8) insulin does not exhibit cold-induced aggregation, as monitored by UV difference and CD spectra. The following dynamic exchange phenomena are observed. The ring resonances of HisB5 broaden between 0 and 20 °C, suggesting intermediate exchange between different ring configurations (as indicated by an asterisk at resonance b in the bottom panel). Such broadening is not observed for HisB10 under monomeric conditions. Disproportionate broadening is also observed in the resonances of PheB24 (asterisk at resonance i) and TyrA19. Some broadening is also observed between 0 and 10 °C in the resonances of TyrB26, which also shift upfield. Resolution was enhanced by convolution difference with parameters of 2 and 4 Hz and a subtraction ratio of 1.0.

20 as a function of the percentage of acetic acid–sodium acetate (pD 3.0) in the solution. At a level of 20% the protein is substantially (95%) monomeric under these conditions (1 mM insulin at 37 °C), and three enhancements are observed, assigned as above to A14, B16, and B26 (panel D). The polarization of the B-chain tyrosines is reduced relative to that observed at pD 1.8 (Figure 15) due to partial dimerization. This is presumably due to shielding of B16 and B26 in the dimer interface. The effect of such shielding is more complete as the percentage of acetic acid–sodium acetate is reduced, favoring self-association (panels C–A). TyrB16, but not TyrB26, exhibits some residual polarization under oligomeric conditions (as indicated by an arrow in panel B). This is consistent with the partial exposure of TyrB16, but not TyrB26, in the crystallographic dimer (Table III).

(*v*) *Conformational Substrates.* The ^{1}H NMR spectrum of insulin exhibits large variations in resonance line widths. This is most apparent in the amide region and presumably arises from an equilibrium among conformational substates [part II(i)]. Experiments designed to assign these broadened resonances by isotopic labeling and to measure the exchange rates by determination of selective $T_{1\rho}$ relaxation times are in progress. This hypothesis may be further examined through studies of an insulin analogue containing a peptide bond between residues LysB29 and GlyA1 (mini-proinsulin). In the two-Zn crystal B29 and A1 are in close proximity (Blundell et al., 1971), and so the B29–A1 peptide bond may locally constrain the protein to adopt a conformation similar to that observed in the crystal. Indeed, this analogue has been shown

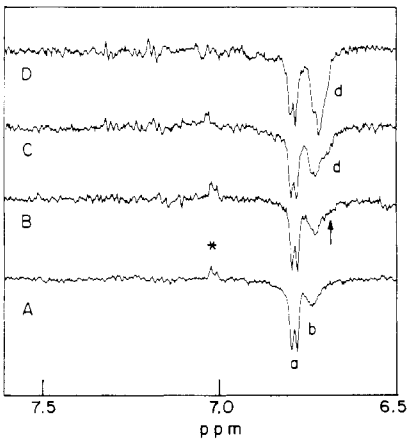

FIGURE 20: Photo-CIDNP difference spectra of human insulin are shown as a function of the percentage of acetic acid in solution in the range 0–20% at pD 3.0 and 37 °C. The protein concentration was 1 mM. At 20% acetic acid–sodium acetate (panel A) three enhancements are observed, assigned to TyrA14 (resonance a), TyrB16 (resonance b), and TyrB26 (resonance d; see Figures 16–18). The polarization of the B-chain tyrosines is less than that observed at pD 2.2, consistent with shielding due to partial dimerization. This attenuation of photo-CIDNP enhancement becomes progressively more marked as the percentage of acetic acid–sodium acetate is reduced (panels B–D). The polarization of TyrA14 is not affected. More shielding is observed for TyrB26 than for TyrB16, as indicated by an arrow in panel C. This is consistent with accessibility calculations based on the structure of the dimer in the two-Zn crystal (Table III). The asterisk in panel A indicates a transfer of polarization from the 3,5 to 2,6 ring protons of TyrA14; it is positive in the difference spectrum due to the segmental mobility of TyrA14. These difference spectra were processed with 2-Hz exponential multiplication for sensitivity enhancement.

Table III: Solvent and Dye Accessibility (Å^2) of the Hydroxyl Groups of the Tyrosine Residues[a] in the Insulin Monomer (m) and Dimer (d)

		A14[b]		A19		B16		B26	
		m	d	m	d	m	d	m	d
1.6 Å	radius probe								
	molecule 1	12.0	12.0	1.2	0.1	10.7	5.7	2.8	1.3
	molecule 2	12.0	12.0	6.6	2.6	10.8	5.9	2.9	0.8
4.0 Å	radius probe[c]								
	molecule 1	9.0	9.0	0.1	0.1	8.4	3.1	0.2	0.0
	molecule 2	9.0	9.0	2.6	2.6	7.3	1.9	0.4	0.0

[a] Accessibility was calculated by the method of Richards (1975) based on the two-Zn crystal model of porcine insulin (Blundel et al., 1971). The accessibility of the hydroxyl of free tyrosine to a 1.6-Å probe is 12.0 Å^2 and to a 4-Å probe is 9.0 Å^2. [b] PheB1 partially covers TyrA14 in the crystal, reducing its calculated accessibility; it was deleted in the calculations shown above. Including PheB1, the accessibility of the TyrA14 hydroxyl to a 1.6-Å probe is 7.3 and 6.4 Å^2 in molecule I and molecule II, respectively; its accessibility to a 4-Å probe is 3.9 Å^2 in both subunits. [c] Because photo-CIDNP effects depend on the productive collision of the dye (riboflavin) with the tyrosine hydroxyl, a larger probe size was simulated.

to fold properly and to form zinc crystals under the same conditions as does native insulin (Markussen, 1985a,b).

The aromatic NMR spectrum of mini-proinsulin (0.5 mM) is shown in panel A of Figure 21 at 37 °C and pD 1.8. Residues B10 and B24–B26 (indicated by asterisks) are broadened by intermediate exchange, and the photo-CIDNP enhancement of the B-chain tyrosines is substantially reduced (panel C). These features imply that mini-proinsulin is forming dimers and higher-order oligomers under conditions in which native insulin is monomeric. The B29–A1 peptide bond is presumably constraining the protein into a conformation favorable for self-association. Such an effect is not observed for native proinsulin, which is monomeric even at 2 mM and pD 3 (panels C–E in Figure 21). The near-UV

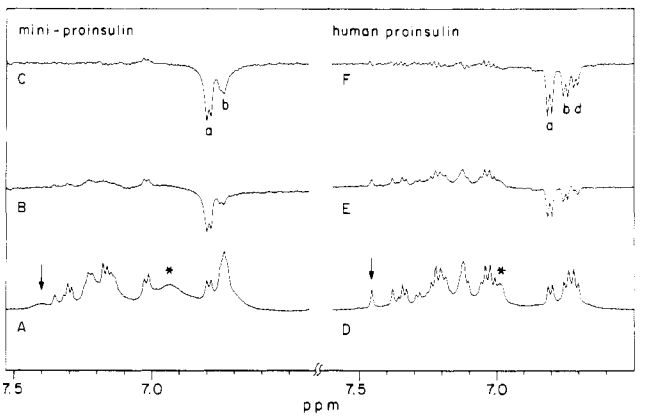

FIGURE 21: Aromatic region of the ^{1}H NMR spectra of B29-A1 single-chain insulin (mini-proinsulin) at 37 °C at pD 1.8 (panel A) demonstrates a pattern of broadening indicative of dimer and hexamer formation. Photo-CIDNP studies of this analogue (panels B and C) demonstrate partial shielding of the B-chain tyrosines under these conditions, which provides additional evidence for dimerization. In contrast, native proinsulin is monomeric under these conditions, as shown by the corresponding data in panels D–F. The asterisks in panels A and D indicate resonances assigned to the ortho protons of PheB24 and TyrB26; their line width is sensitive to dimerization. The arrows in panels A and D point to the C_4H resonance of HisB10, whose line width is sensitive to hexamer formation. The concentration of B29-A1 single-chain insulin was 0.5 mM; the concentration of human proinsulin was 2 mM. The spectra shown in panels A and D were processed without weighting functions; those in panels B, C, E, and F were processed with 2-Hz exponential multiplication for sensitivity enhancement.

regions of the CD spectra of insulin, mini-proinsulin, and proinsulin also show a pattern consistent with enhanced dimerization of the cross-linked analogue but not of proinsulin (data not shown).

Like B29–A1 insulin, proinsulin is a single-chain protein. Its "cross-link" consists of a connecting peptide of 35 residues, which presumably is too flexible to constrain the conformation of the B-chain. In fact, the amide resonances of proinsulin exhibit a pattern of differential broadening similar to that of insulin, which suggests that the connecting peptide does not damp the motions involved. A detailed NMR study of proinsulin will be published separately.

(IV) Rigid Rotation Maps

Steric hindrance to ring rotation may be examined by calculation of the energy of a protein as a function of side-chain configuration (Gelin & Karplus, 1975). The results of such calculations are displayed as contour maps of total potential energy. The energy is the sum of van der Waals and electrostatic terms in a rigid structure; the effects of adiabatic minimization are not included (Karplus, 1987). Since the calculations are based on the crystal structure, these provide qualitative insights which avoid artifacts associated with the use of energy minimization procedures (Shih et al., 1985).

A quantitative calculation of the local potential energy surface must allow the system to relax at each configuration examined (adiabatic maps). Since unfavorable local interactions can often be dissipated by adjustments of other side chains, barriers between local minima are overestimated by the rigid calculation. A rigid barrier of <5 kcal/mol, for example, is usually associated with free ring rotation at room temperature. Quantitative calculations are time-consuming, however, and qualitative insights may be provided by the simpler procedure.

In this part rigid maps are presented for each aromatic ring. The relation between the calculated and observed features of the ring dynamics are analyzed under Discussion. These

calculations are based on the two-Zn structure of porcine insulin refined at 1.5 Å (Blundell et al., 1971). The difference between porcine and human insulins (AlaB30 → Thr) is unlikely to influence these calculations.

HisB5. In the two-Zn structure the configuration of HisB5 differs in molecule I and molecule II. The side-chain rigid rotation map calculated for molecule I is shown in panel A of Figure 22. The configuration observed in molecule I (indicated by an X in the figure) is −74.7,94.7, and the imidazole appears to be singly protonated at N_{δ_2}. There is a single minimum in the potential energy surface, stabilized by a hydrogen bond between N_{δ_2} and the carbonyl of CysA7. Ring rotation around χ_2 is hindered by contacts involving the main-chain atoms of CysA7, ThrA8, and SerA9.

The configuration of HisB5 observed in molecule II is 179.4,39.1. Unlike its state in molecule I, HisB5 appears to be protonated at N_{ϵ_1} as well as N_{δ_2} in molecule II. Rigid maps calculated for molecule II are shown in panel C (singly protonated at N_{δ_2}) and panel D (doubly protonated) in Figure 22. In the first case there are three minima with different χ_2 values. The χ_1 value is restricted in a trans conformation. The transition from χ_2 from 60° to 120° is separated by an energy barrier of less than 6.0 kcal/mol. The χ_2 transition from the g^+ to g^- conformation is separated by an energy barrier of more than 17.0 kcal/mol. Similar features are observed by assuming double protonation (panel D). The observed configuration is in the vicinity of the global minimum, and there are three additional minima. The latter are more than 10.0 kcal/mol less favorable than the global minimum. As described for molecule I, the configuration of HisB5 is constrained by neighboring atoms in the A-chain.

HisB10. This residue is exposed to solvent and has no neighbor constraining its configuration. Its configuration in both molecule I and molecule II is g^-,g^+ and is apparently stabilized by zinc coordination. Its calculated rigid map is shown in panel B of Figure 22. In the absence of zinc the apparent energy barrier to rotation about χ_2 is less than 4.0 kcal/mol. The ring is thus expected to be free to rotate in solution. In addition, χ_1 can adopt a wide range of values from −180.0° to −60.0°. The rigid map of HisB10 exhibits many local minima, which are separated by apparent barriers of less than 10.0 kcal/mol. These calculations suggest that in the monomer HisB10 can undergo considerable side-chain motion.

PheB1 is located near the aromatic ring of TyrA14 and the side chain of LeuA13. Its rigid map (panel E of Figure 22) contains two minima at −60,−60 and −60,−120 related by the symmetry of the ring around the C_β–C_γ bond axis. The calculated barrier to ring rotation of 320 kcal/mol is largely due to van der Waals contacts between the ring and the B1 amino group. Since the latter is itself not otherwise constrained, the actual barrier is likely to be negligible. Such motions of the N-terminus and B1 ring are observed in molecular dynamics simulations (unpublished results).

PheB24. This residue is partially buried inside the protein. An interaction is observed with TyrB16, LeuB15, and the A20–B19 disulfide. One set of symmetry-related minima are observed in the rigid map (panel F of Figure 22). This configuration is g^+,g^- and corresponds to that observed in the two-Zn structure, as indicated by an X in the figure. Rotation around χ_2 is hindered by the close contacts described above.

PheB25 has different χ_1 values in molecule I and molecule II. In monomer I the aromatic ring of PheB25 projects inward and interacts with the ring of TyrA19. It also comes into contact with the O_γ of AsnA21. In monomer II the ring projects into the solution and does not interact with any atoms

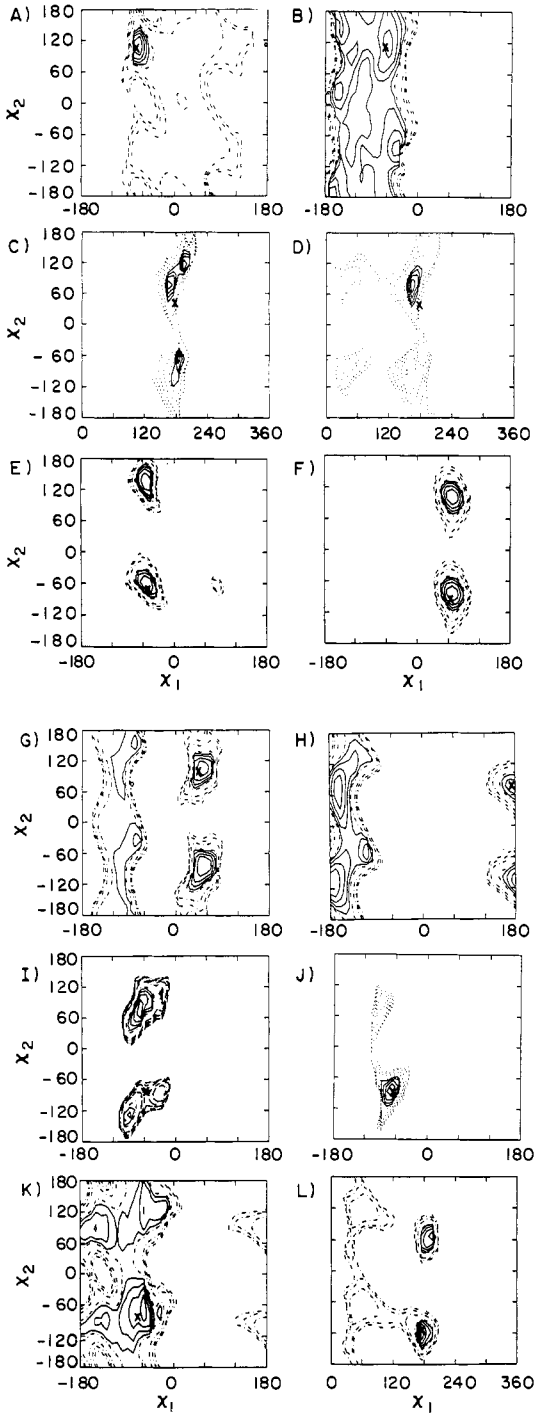

FIGURE 22: Potential energy surface generated by the χ_1 and χ_2 rotations of an aromatic ring is modeled by rigid rotation maps. The C_α–C_β–C_γ–N_{δ_2} atoms were used to define the χ_2 dihedral angle of histidine. These maps are based on the two-Zn structure of porcine insulin, molecule I being used unless otherwise noted. The solid lines represent contours at energy levels of 0, 2, 4, 6, and 8 kcal/mol relative to the local minimum; the dotted lines represent contours at 10, 15, 20, 25, and 30 kcal/mol. (A) HisB5 in molecule I; (B) HisB10 in molecule I; (C) HisB5 in molecule II in which the histidine ring is singly protonated at N_{δ_2}; (D) HisB5 in molecule II in which the histidine ring is protonated at N_{ϵ_1} in addition to N_{δ_2}; (E) PheB1; (F) PheB24; (G) PheB25; (H) TyrA14; (I) TyrA19; (J) TyrA19; (K) TyrB16; (L) TyrB26.

from its own protomer. In this configuration the ring stacks upon the neighboring PheB25 in the dimer interface. The rigid map displays different features in the neighborhood of these two configurations (panel G). In the inward configuration (molecule I) rotation around χ_2 is restricted by intramolecular packing (apparent barrier height of approximately 80 kcal/

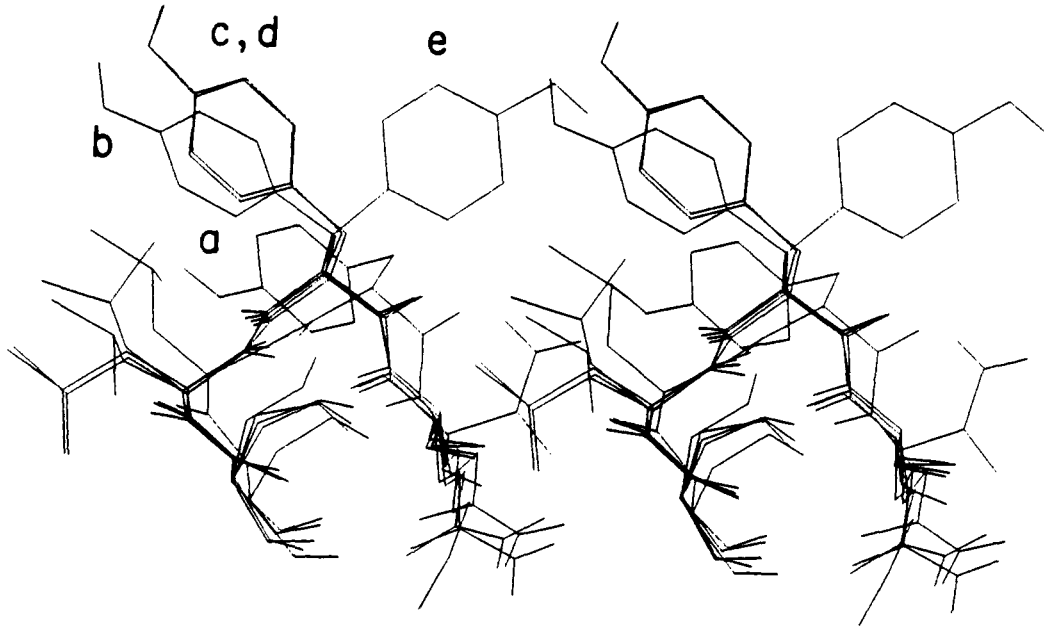

FIGURE 23: TyrA14 exhibits a variety of side-chain configurations in different crystal forms of porcine insulin (Baker et al., 1988). The following crystal structures of insulin were aligned to minimize the root-mean-square differences between the main-chain atoms of residues A13–A15: (a) four-Zn molecule II (Bentley et al., 1976), (b) two-Zn molecule II (Blundell et al., 1971), (c) two-Zn molecule I (Blundell et al., 1971), (d) cubic (Caves and Dodson, personal communication), and (e) four-Zn molecule I (Bentley et al., 1976) crystal forms.

mol), which includes contributions from the main-chain atoms of TyrA19 and TyrB26. In contrast, the corresponding barrier in the outward configuration (monomer II) is less than 4.0 kcal/mol and is unlikely to be significant.

TyrA14 projects into solution and is near the side chains of LeuA13 and GluA17. TyrA14 adopts a wide range of conformations in various different insulin crystal structures, as is illustrated in Figure 23. Its rigid map (panel H of Figure 22) suggests that χ_2 rotation is unrestricted (apparent barrier <6.0 kcal/mol). Variations of 60° in χ_1 are also accessible, consistent with large-amplitude fluctuations in ring position.

TyrA19. LeuB15, LeuA16, and IleA2 form a hydrophobic floor of a crevice in which the TyrA19 ring is located. The environment of TyrA19 differs in molecule I and molecule II. This is due in part to the change in the configuration of PheB25 (see Above). In addition, in molecule I the *p*-hydroxy group forms a hydrogen bond with the side chain of GlnA5; this hydrogen bond is not observed in molecule II. TyrA19 appears to be more flexible in molecule II than in molecule I on the basis of an analysis of *B* factors in the X-ray structures. Rigid maps calculated for molecule I (panel I) and for molecule II (panel J) exhibit one set of symmetry-related minima. Due to the asymmetry of the *p*-hydroxy group, one minimum has a lower relative energy than the other. Ring rotation about χ_2 is restricted by contacts with methyl groups in the floor of the crevice. The calculated barrier is also influenced by the position of PheB25: the barrier is greater than 120 kcal/mol when PheB25 projects inward and less than 40 kcal/mol when PheB25 projects outward.

TyrB16 projects into solution. Its rigid map is shown in panel K of Figure 22. A wide range of χ_2 values (−180 to −50) are accessible (relative energy 6 kcal/mol), and rotation about χ_2 is unrestricted (apparent barrier <8.0 kcal/mol, due largely to its own main chain).

TyrB26 is partially buried. One side of the ring packs against the methyl groups of ValB12; the other side packs against ProB28. When χ_1 adopts the trans configuration, as observed in the two-Zn structure, rotation about χ_2 is restricted by van der Waals contacts between the ring and the methyl groups of ValB12 (apparent barrier greater than 260 kcal/mol). However, rotation of χ_1 to 120° reduces this barrier to less than 10 kcal/mol. In this configuration the B26 ring projects into solution, permitting unrestricted ring rotation. The trans configuration provides favorable van der Waals interactions (20 kcal/mol), which are absent in the outward configuration. Such stabilization would also be reduced by motions involving ProB28 as described in a molecular dynamics simulation of the insulin monomer (Kruger et al., 1987).

Discussion

The primary objective of this paper is the assignment and analysis of the aromatic ^{1}H NMR spectrum of the insulin monomer. These resonances provide probes for structure, self-association, and dynamics in solution. There are four tyrosines, three phenylalanines, and two histidines. The histidines have previously been assigned (Bradbury et al., 1980). One-dimensional assignment of the tyrosine resonances at pH 10–12 has also been reported (Bradbury & Ramesh, 1985); the assignments are consistent with those obtained in the present analysis. Our two-dimensional NMR assignments have been obtained by comparative studies of genetically altered and chemically modified variants. Under conditions used here sequential assignment strategies (Wuthrich et al., 1983) were found to be difficult to apply due to variations in amide line widths.

Characterization of Conditions

Our studies have been performed under acidic conditions to reduce higher-order aggregation (Jeffrey & Coates, 1966a,b; Cheshnovsky et al., 1983). The increased net positive charge of the protein under acidic conditions increases the dissociation constant (K_d) from 1 μM (pH 7.4) to 0.1 mM (pH 2.0) (Jeffrey & Coates, 1966a). Titration of individual groups, such as the six carboxylates from GluB13 in the hexamer interface, may specifically destabilize self-association. The CD spectrum of insulin is unperturbed in this range (Pocker & Biswas, 1980). To weaken dimerization further, insulin was investigated as a function of acetic acid concentration. In 20% acetic acid the protein was found to be monomeric at the millimolar concentrations required for NMR study. This

mixed-solvent system presumably weakens hydrophobic interactions between monomers. Assuming that 5% dimerization would have been detected by optical or NMR spectroscopy, the absence of observable dimerization at 2 mM protein concentration (in 20% acetic acid at pH 2.0) places a lower limit of 72 mM on the dissociation constant (K_d). In 20% acetic acid–sodium acetate (pH 3.0) approximately 5% dimer was observed at 37 °C at an insulin concentration of 0.5 mM, implying that the dissociation constant under these conditions is 18 mM.

Tertiary structure is retained under these conditions, as indicated by (i) the dispersion of ^{1}H NMR resonances, (ii) nonlocal effects of chemical modification or site-specific mutagenesis, and (iii) the inaccessibility of TyrA19 to photo-CIDNP enhancement. The 1D NMR spectrum exhibits features similar to those described at pH 10–12 in aqueous solution (Bradbury & Ramesh, 1985). These include the unusual broadening of PheB24, an unassigned feature attributed to an impurity in the earlier work.

Aggregation State and Specific Protein–Protein Interactions

(*i*) *Intermediate-Exchange Broadening.* We have observed that the protein surfaces necessary for self-association are intact in 20% acetic acid (pD 3). Specific B-chain dimerization is observed with increased protein concentration or decreased temperature and may be monitored by broadening of the resonances assigned to the dimer site. These include TyrB16, PheB24, PheB25, and TyrB26. At higher protein concentrations broadening is also observed in the resonances of HisB10. We attribute this to higher-order oligomerization, since HisB10 lies near the 3-fold axis in the crystallographic hexamer. Loss of self-association occurs with increasing temperature in the range 0–45 °C. At temperatures higher than 45 °C the monomer gradually unfolds, resulting in exposure of TyrA19 to photo-CIDNP enhancement (below) and reduction in chemical shift dispersion.

(*ii*) *Photo-CIDNP.* Photo-CIDNP enhancements may be used to monitor the environments of tyrosine rings during the monomer–dimer transition. Because tyrosine residues are involved in dimerization (Blundell et al., 1971), the pattern of enhancements changes with the state of insulin aggregation. In the monomer three enhancements are observed, assigned (in order of polarization intensity) to A14, B16, and B26. With dimerization the enhancement of B16 and B26 diminishes, consistent with their position in the dimer interface. In the dimer B26 is also less accessible to photo-CIDNP enhancement than B16. These observations extend a previous photo-CIDNP study of bovine insulin at 270 MHz (Muzskat & Gilon, 1978; Muzskat et al., 1984). One resonance (assumed to be that of TyrA14) was enhanced under conditions favoring formation of dimers and higher-order oligomers.

The photo-CIDNP effect requires collision between the triplet-state dye and an accessible tyrosine hydroxyl group, which leads in turn to formation of a radical pair (Kaptein, 1980). The observed results may be compared with probe accessibilities (Richards, 1975) calculated from the two-Zn crystal structure. The results of this calculation are given in Table III. The entries represent the contribution of each tyrosine hydroxyl group to the surface (in squared angstroms) accessible to a sphere of given radius. A radius of 1.6 Å corresponds to that of water; a radius of 4 Å approximates the effective dimension of riboflavin. Calculated accessibilities can depend on probe size; for example, crevices accessible to a smaller probe may be inaccessible to a larger probe (Novotny & Broccoleri, 1987).

Four conclusions emerge from this analysis: (i) The CIDNP enhancement of A14 would not be predicted by a static analysis of the insulin monomer in the two-Zn structure, since PheB1 is positioned to limit the accessibility of the A14 hydroxyl. Thus, the observed enhancement of A14 provides evidence that the A14–B1 interaction is not stably maintained in solution. This interaction is not observed in molecule II of the four-Zn structure (Dodson et al., 1984) nor in frames taken from molecular dynamics simulations of the two-Zn monomer (Kruger et al., 1987); in these cases PheB1 is displaced from its position in the two-Zn structure, and the A14 hydroxyl is fully accessible to solvent. Alternative configurations of A14 are observed in various crystal structures, as shown in Figure 23. (ii) The enhancement of TyrB16 in the monomer and its attenuation in the dimer are consistent with the calculated accessibilities. (iii) The absence of A19 enhancement is consistent with its position in a hydrophobic pocket. Although accessible to water (indeed, solvent molecules are observed in this pocket in the two-Zn crystal), accessibility to the large probe is limited. (iv) The significant enhancement exhibited by B26 is inconsistent with the calculated accessibilities in the static structure. However, small changes in side-chain configuration would allow exposure of the hydroxyl group; such flexibility is discussed further below.

Conformational Substates

Conformational flexibility has previously been inferred from structural differences observed in various crystal states (Chothia et al., 1983). Evidence for an equilibrium among conformational substates is provided by the observation of large variations in amide line widths. Since these variations are not due to solvent exchange, a structural mechanism is suggested; i.e., the existence of a range of conformations with different chemical shifts that are incompletely averaged on the NMR time scale (Anasari et al., 1985; Elber & Karplus, 1987). This interpretation is supported by the observation of more extensive line broadening at higher field strengths (shifting the NMR time scale) and, conversely, of less extensive line broadening in partial proteolytic fragments (shifting the frequencies of internal motions involved).

Additional evidence for conformational substates is provided by the study of a single-chain insulin analogue (mini-proinsulin) containing a peptide bond between LysB29 and GlyA1 (Markussen, 1985a,b). This bond can be modeled in the two-Zn crystal structure of native insulin with minimal nonlocal distortion. This analogue forms crystals isomorphic to those of native insulin (Markussen, 1985b). Such a cross-link would be expected to constrain the molecule to assume a conformation in solution similar to that observed in the crystal state.

We have demonstrated that the cross-linked protein forms dimers and higher-order oligomers under conditions in which the native molecule is monomeric. Since the residues involved in the cross-link (LysB29 and GlyA1) are not directly involved in dimerization, this implies a nonlocal stabilization of structure favoring formation of the dimer interface. In the absence of the cross-link, we propose that the C-terminal region of the B-chain is flexible and may adopt configurations in which (a) its C-terminus is not near GlyA1 and (b) the configuration of B24–B26 is less favorable for dimerization. This proposal is supported by the anomalous electrophoretic mobility of the B29-A1 analogue seen in earlier studies, which suggested that it adopts a more compact structure than that of native insulin (Markussen, 1985a). Differences in the overall relationship between this region of the B-chain and the A-chain have been described in molecule II of the four-Zn structure (Dodson et

al., 1979; Chothia et al., 1983) and may play an important role in high-affinity receptor binding (Mirmira & Tager, 1989).

Native proinsulin may be regarded as a single-chain analogue whose "cross-link" is a 35-residue connecting peptide between B30 and A1. Variations in amide line widths are observed in its ^{1}H NMR spectrum that are similar to those in the spectrum of insulin (unpublished results). Unlike the B29-A1 analogue, proinsulin does not exhibit an enhancement of dimerization. Presumably, the extended tether provided by the connecting peptide is too flexible to constrain the conformation of the B-chain. These results provide a structural mechanism for the observation that the fully reduced B29-A1 analogue folds more efficiently than proinsulin to form the correct pattern of disulfide bonds (Markussen, 1985b).

Local Dynamics

Insulin is observed to display a variety of local structural and dynamic features. In this section the observed NMR features of the aromatic resonances are considered individually in relation to their environments in the crystal structures. The experimental side-chain dynamics are also compared with those predicted by the rigid rotation maps described above (part IV).

(*i*) *HisB5* lies on the surface of the protein in a pocket formed by CysA7 and IleA10. The two protomers in the two-Zn crystal exhibit alternate hydrogen-bonding patterns (Blundell et al., 1971) which alter the environments of the H_2 and H_4 ring protons. The rigid maps of these two configurations are shown in panels A, C, and D of Figure 22. Large barriers are observed, and the most accessible path appears to involve changes in both χ_1 and χ_2. These calculations are consistent with the observed features of HisB5. In the monomer the resonances of HisB5 are broader than those of HisB10, and NOEs provide evidence for stable packing interactions. With decreasing temperature the resonances of HisB5 disproportionately broaden in the monomer. This broadening is presumably due to intermediate exchange among alternative ring configurations. From 40 to 0 °C such exchange goes from fast to intermediate on the NMR time scale. Under the acidic conditions used in the present NMR study, HisB5 is doubly protonated and thus able to participate in the alternative hydrogen-bonding schemes observed in the crystal.

(*ii*) *HisB10* projects outward from the surface of the B-chain α-helix and coordinates zinc in the hexamer. There are few intramolecular contacts which would constrain its motion. In the rigid map (panel B of Figure 22) there is a broad region accessible to the ring with $-180° < \chi_1 < -40°$ and no significant barriers for χ_2 rotation. This is consistent with the absence of significant interresidue NOEs. With increasing protein concentration the resonances of HisB10 are observed to broaden. This is likely to represent intermediate exchange related to higher-order oligomerization and reflects the position of B10 in the tetramer/hexamer interface.

(*iii*) *PheB1 and TyrA14.* Electron density for these residues is well-defined in the crystal state, and in the two-Zn model an A14–B1 interaction is observed (Blundell et al., 1971). The narrow line widths (T_2 relaxation) of PheB1 and TyrA14 suggest that these residues are flexible in solution. No perturbation in B1 is seen following chemical modification of TyrA14, and no NOE is observed between these rings. These results indicate that the A14–B1 interaction in the two-Zn crystal is unlikely to be maintained in solution. A similar conclusion has been reached on the basis of near-UV circular dichroism studies of a des-PheB1 analogue (Wollmer et al., 1979). The CD spectra of native insulin and des-PheB1-insulin were shown in that study to be identical; the significant contribution expected of the A14–B1 complex (if maintained in solution) was not observed. The rigid map of B1 does show significant barriers to ring rotation (panel E of Figure 22). These are almost entirely due to the presence of the N-terminal amino group, however, and are not seen in a dynamic model in which barriers to ring rotation were not explicitly evaluated (Kruger et al., 1987). The flexibility of TyrA14 is consistent with its rigid map (panel H of Figure 22) and with the variety of side-chain configurations observed in different crystal forms (Figure 23).

(*iv*) *PheB24* projects into the hydrophobic interior and packs against LeuB15 on one side and the A20–B19 disulfide on the other. Large barriers for ring rotation are calculated due to these groups and also to the presence of TyrB16 (panel F of Figure 22). Such barriers are consistent with the unusual broadening of the PheB24 resonances in solution. These features can also arise from more extended motions [e.g., ring sliding (McCammon et al., 1979)]. The apparent broadening of the para resonance suggests the involvement of χ_1, since this proton is on-axis for C_β–C_γ rotation.

(*v*) *PheB25* is observed in two configurations in the crystallographic monomer. These are related by a large change in χ_1 ($\Delta\chi_1 = 120°$). In molecule I PheB25 projects inward, where it interacts with TyrA19. In molecule II PheB25 projects outward to contact the other protomer and does not make any significant intramolecular contacts. These two states occur in different regions of the rigid map (panel G of Figure 22). In the inward configuration (molecule I) a local minimum is well-defined, and there are significant barriers to ring rotation. In the outward configuration (molecule II) no significant barriers in χ_2 are calculated, and variations in χ_1 of 80° are permitted. These configurations give rise to different predictions of which NOEs would be nonnegligible (Figure 14 and Table II). The inward configuration predicts an interaction between the A19 and B25 rings in solution, which is not observed. Moreover, chemical modification of A19 does not perturb the resonance of B25, although perturbations are seen in B24 and B26. These results imply that PheB25 is not stably packed against TyrA19 in solution. However, the alternative configuration predicts an interaction between B25 H_{β_2} and an ortho proton of A19, which is also not observed. This interaction would be weakened significantly by variations in χ_1; such averaging has in fact been observed in a molecular dynamics simulation of molecule II (unpublished results). Flexibility in the outward configuration is consistent with the NMR features of PheB25, including the absence of predicted NOEs, resonance line width, and chemical shift.

(*vi*) *TyrA19* projects into a hydrophobic crevice, where it packs against IleA2, LeuA6, and LeuB15. A well-defined minimum is observed in the neighborhood of the configuration found in the crystal, and significant barriers to displacement in χ_1 or χ_2 are seen. The broadening of the A19 resonances at lower temperature may reflect such barriers. Alternatively, more extended motions (e.g., ring swinging) are suggested by the asymmetric pattern of B values among ring atoms in two-Zn molecule II (Baker et al., 1988). In the A19 pocket the side of the ring exposed to solvent exhibits higher B values than the side interacting with IleA2. The stable packing of TyrA19 within the crevice is consistent with the strong NOEs observed between the ring and several methyl resonances, including those of IleA2 (data not shown).

(*vii*) *TyrB16* projects from the surface of the B-chain α-helix and participates in dimer interactions. The rigid map (panel K of Figure 22) demonstrates no significant barriers to ring rotation in the monomer, and 60°–80° variations is χ_1 are also

permitted. These calculations are consistent with the narrow line width of B16 in the insulin monomer at all temperatures studied.

(*viii*) *TyrB26* lies in a hydrophobic pocket of the protein, exposed to solvent on one side and involved in hydrophobic interactions on the other. This pocket is formed primarily by IleA2, ValA3, ValB12, and LeuB15. These residues are highly conserved (Pullen et al., 1976). On the other side TyrB26 packs against ProB28. This configuration is stabilized in the two-Zn crystal by an interaction with dimer-related PheB24. The rigid map (panel L of Figure 22) demonstrates a well-defined minimum in the neighborhood of the crystallographic configuration with significant barriers to ring rotation. These barriers are due to both the aliphatic chains on one side and ProB28 on the other. These static features are inconsistent with the fast-exchange features of B26 at 37 °C. However, it is possible to rotate TyrB26 out of its pocket ($\Delta\chi_1 = 60°$), and in this configuration rotation about χ_2 is possible. Such rotation exposes the B26 hydroxyl group to solvent, accounting for its observed photo-CIDNP enhancement. Displacement of ProB28 also increases the configurations accessible to TyrB26. At low temperatures the B26 resonances are observed to broaden. This may reflect local stabilization within the B26 pocket.

Nonlocal displacement of the B24–B30 region has been proposed to occur in the hormone–receptor complex (Dodson et al., 1979; Baker et al., 1988). Such displacement could expose the underlying hydrophobic surface (including IleA2 and ValA3), enabling these residues to interact directly with the receptor. This model is in accord with the strict conservation of this surface (in contrast to evolutionary divergence exhibited by residues B26–B30) and would rationalize the anomolous binding properties of B24 and B25 analogues, including the retention of full activity by des-pentapeptide-insulin amide (Mirmira & Tager, 1989). Comparative NMR studies of insulin analogues designed to probe further the dynamics of this region and its relationship to the conserved hydrophobic surface are in progress.

Conclusions

The physiologically active form of insulin is the monomer. By monitoring dimerization with circular dichroism and UV difference spectroscopy, conditions have been determined at acidic pH for the NMR study of insulin in the monomeric state; these conditions are 20% acetic acid (pH 2.2). Control CD and NMR experiments demonstrate that insulin retains native-like structure under these conditions. The aromatic NMR resonances of monomeric insulin have been completely assigned by a combination of site-directed mutagenesis and chemical modification. The two histidine, three phenylalanine, and four tyrosine residues are observed to be in distinct local environments; their assignment provides sensitive markers for tertiary structure and protein dynamics. The environments of the tyrosine residues have also been investigated with photochemically induced dynamic nuclear polarization (photo-CIDNP).

Comparison of the observed features with computer-based modeling of packing constraints in the crystal structures of insulin led to the following conclusions. (i) The observed pattern of nuclear Overhauser enhancements and resonance line widths is in qualitative agreement with that expected from the crystal structure. The chemical shift, line width, and NOE pattern of PheB25 indicate that its configuration is more like that observed in molecule II (externally rotated) than that in molecule I (internally rotated) in the crystallographic hexamer. (ii) HisB10 is flexible in solution, whereas HisB5 is constrained by several intramolecular contacts. At low temperatures the resonances of HisB5 selectively broaden, indicating intermediate exchange between different local environments; this may correlate with the alternative configurations and hydrogen-bonding schemes observed for HisB5 in the crystal state. (iii) Barriers to ring rotation are observed for PheB24 and TyrA19, whose tertiary interactions are highly conserved. A19 is the only tyrosine in the monomer which is inaccessible to photo-CIDNP enhancement in the native state; enhancement of A19 is observed upon thermal denaturation. (iv) In the monomer differences between observed and calculated features are observed near the N-terminus (PheB1) and C-terminus (TyrB26) of the B-chain, which appear to be more flexible in solution than in the crystal state. Such flexibility would account for the significant photo-CIDNP enhancement exhibited by TyrB26. (v) Dimerization involving specific B-chain interactions is observed with increasing protein concentration, decreasing temperature, or increasing pH; under these conditions the resonances of B16, B24, B25, and B26 broaden. In addition, TyrB16 and TyrB26 become progressively less accessible to photo-CIDNP enhancement, consistent with their positions in the crystallographic interface. With additional self-association the resonances of HisB10 also broaden, presumably reflecting formation of tetramers and hexamers. (vi) Large variations are observed in the line widths of amide resonances, suggesting intermediate exchange between conformational substates; such substates may relate to conformational changes observed in different crystals or to changes in the conformation of the C-terminal region of the B-chain proposed to accompany receptor binding. (vii) One set of substates is stabilized by a peptide bond between residues B29 and A1. This leads to enhanced formation of dimers and higher-order oligomers in the single-chain analogue (mini-proinsulin). Such stabilization is not observed in corresponding studies of native proinsulin. Since reduced mini-proinsulin folds more efficiently than native proinsulin to form the correct pattern of disulfide bonds, the B29–A1 peptide bond is likely to stabilize interactions involved in the pathway of nascent protein folding.

These NMR studies have provided information regarding overall and local flexibility of the insulin monomer. Such motions may play a central role in formation of the hormone–receptor complex. In the future the functional role of the observed NMR features will be evaluated by comparative study of mutant insulins with enhanced or diminished affinity for the insulin receptor, including those associated with diabetes mellitus in man.

Acknowledgments

NMR spectra were obtained at the MIT High Field NMR Resource (Grant RR-00995) and the University of Wisconsin NMR Facility (RR-02301 and NSF Grant PCM-8415048). We thank Ad Bax (NIH) and George Gray (Varian, Inc.) for helpful discussion and instrument time, Dennis Torchia for helpful discussion, Ron Chance (Lilly Research Laboratories) for insulin analogues, J. Markussen (Novo Pharmaceuticals, Denmark) for the single-chain B29-A1 insulin analogue, L. Caves and Prof. G. Dodson for communication of the coordinates of cubic insulin prior to publication, Jeff Hoch and Alan Stern (Rowland Institute for Science, Cambridge, MA) for ring current shift calculations, Alan Pekar (Eli Lilly) for assistance with CD measurements, and Peter Kim (MIT) for use of his CD spectrophotometer. S.E.S. thanks C. Ronald Kahn for laboratory space and helpful discussions. M.A.W. and S.E.S. thank Prof. Eugene Braunwald and Prof. John Potts, Jr., for their encouragement.

Registry No. L-His, 71-00-1; L-Phe, 63-91-2; L-Tyr, 60-18-4; insulin, 9004-10-8; human insulin, 11061-68-0; mini-proinsulin, 98745-24-9; mutant insulin (PheB25 → Leu), 78564-74-6.

REFERENCES

Adams, M. J., Blundell, T. L., Dodson, E. J., Dodson, G. G., Vijayan, M., Baker, E. N., Hardine, M. M., Hodgkin, D. C., Rimer, B., & Sheet, S. (1969) *Nature (London) 224*, 491–495.

Anasari, A., Berendze, J., Bowne, S. F., Frauenfelder, H., Iben, I. E. T., Sauke, T. B., Shyamsun, E., & Young, R. D. (1985) *Proc. Natl. Acad. Sci. U.S.A. 82*, 5000–5004.

Baker, E. N., Blundell, T. E., Cutfield, G. S., Cutfield, S. M., Dodson, E. J., Dodson, G. G., Hodgkin, D. M. C., Hubbard, R. E., Iassac, W. M., Reynolds, D. C., Sakabe, K. S., Sakabe, N., & Vjayan, N. M. (1988) *Philos. Trans. R. Soc. London B319*, 389–456.

Bentley, G., Dodson, E., Dodson, G., Hodgkin, D., & Mercola, D. (1976) *Nature (London) 261*, 166–168.

Berliner, L. J., & Kaptein, R. (1981) *Biochemistry 20*, 799–807.

Blundell, T. E., Cutfield, J. F., Cutfield, S. M., Dodson, E. J., Dondson, G. G., Hodgkin, D. C., Mercola, D. A., & Vijayan, M. (1971) *Nature (London) 231*, 506–511.

Blundell, T. L., & Humbel, R. E. (1980) *Nature (London) 287*, 781–787.

Bradbury, J. H., & Wilairiat, P. (1967) *Biochem. Biophys. Res. Commun. 29*, 84–89.

Bradbury, J. H., & Brown, L. R. (1977) *Biochemistry 16*, 573–582.

Bradbury, J. H., & Ramesh, V. (1985) *Biochem. J. 229*, 731–737.

Bradbury, J. H., Ramesh, R., & Dodson, G. (1981) *J. Mol. Biol. 150*, 609–613.

Brooks, B. R., Bruccoleri, R. E., Olafson, B. O., States, D. J., Swaminathan, S., & Karplus, M. (1983) *J. Comp. Chem. 4*, 187–217.

Brown, H., Sangar, F., & Kitai, R. (1955) *Biochem. J. 60*, 556–565.

Brunger, A. T., & Karplus, M. (1988) *Proteins 4*, 151–176.

Cahill, R., Jr. (1971) *Diabetes 20*, 785–799.

Cheshnovsky, D., Neuringer, L. J., & Williamson, K. L. (1983) *J. Protein Chem. 1*, 335–339.

Chothia, C., Lesk, A. M., Dodson, G. G., & Hodgkin, D. C. (1983) *Nature (London) 302*, 500–505.

Danho, W. O., Gattner, H.-G., Nissen, D., & Zarn, H. (1975) *Hoppe-Seyler's Z. Physiol. Chem. 356*, 1406–1412.

Davis, D. G., & Bax, A. (1985) *J. Magn. Reson. 64*, 533–535.

De Meyts, P., Van Obberghen, E., Roth, J., Brandenburg, D., & Wollmer, A. (1978) *Nature (London) 273*, 504–509.

Dodson, E. J., Dodson, G. G., & Hodgkin, D. C. (1979) *Can. J. Biochem. 57*, 469–479.

Dodson, E. J., Dodson, G. G., Hubbard, R. E., & Reynolds, C. D. (1984) *Biopolymers 22*, 281–291.

Ebina, Y., Leland, E., Jarnagin, K., Eden, M., Lanzlo, G., Clauser, E., Ou, J. H., Masiarz, F., Kan, Y. N., Goldfine, I. D., Roth, R. A., & Rutter, W. J. (1985) *Cell 40*, 747–758.

Elber, R., & Karplus, M. (1987) *Science 235*, 318–320.

Frank, B. H., Peavy, D. E., Hooker, C. S., & Duckworth, W. C. (1983) *Diabetes 32*, 705–711.

Gelin, B., & Karplus, M. (1975) *Proc. Natl. Acad. Sci. U.S.A. 72*, 2002–2006.

Goldman, J., & Carpenter, F. H. (1974) *Biochemistry 13*, 4566–4574.

Haneda, M., Polonsky, K. S., Bergenstal, R. M., Jaspan, J. B., Shoelson, S. E., Blix, P. M., Chan, S. J., Kwok, S. C. M., Wishner, W. B., Zeidler, A., Olefsky, J. M., Freidenberg, G., Tager, H. S., Steiner, D. F., & Rubenstein, A. H. (1984) *N. Engl. J. Med. 310*, 1288–1294.

Hore, P. J. (1983) *J. Magn. Reson. 54*, 539–542.

Horuk, R., Blundell, T. R., Lazarus, N. R., Neville, R. W. J., Stone, D., & Wollmer, A. (1980) *Nature (London) 286*, 822–824.

Inouye, K., Watanabe, K., Tochino, T., Kanaya, T., Kobayashi, M., & Shigeta, Y. (1981) *Experientia 37*, 811–813.

Jeffrey, P. D., & Coates, J. H. (1966a) *Biochemistry 5*, 489–498.

Jeffrey, P. D., & Coates, J. H. (1966b) *Biochemistry 5*, 3820–3824.

Kaptein, R. (1980) in *Photo-CIDNP Studies of Proteins in Biological Magnetic Resonance* (Berliner, W., & Rueben, J., Eds.) Vol. 4, pp. 145–191, Plenum Press, New York.

Karplus, M. (1987) *Ann. N.Y. Acad. Sci. 482*, 255–266.

Kobayashi, M., Ohgaku, S., Iwasaki, M., Maegawa, H., Shigeta, Y., & Inouye, K. (1982) *Biochem. Biophys. Res. Commun. 107*, 329–336.

Kowalsky, A. (1962) *J. Biol. Chem. 237*, 1807–1819.

Kruger, P., Strassburger, W., Wollmer, A., van Gunsteren, W. F., & Dodson, G. G. (1987) *Eur. Biophys. J. 14*, 449–459.

Linde, S., & Hansen, B. (1980) *Int. J. Pept. Protein Res. 15*, 495–502.

Markussen, J. (1985a) *Int. J. Pept. Protein Res. 25*, 431–434.

Markussen, J. (1985b) *Int. J. Pept. Protein Res. 26*, 70–77.

McCammon, J. A., Wolymes, P. G., & Karplus, M. (1979) *Biochemistry 18*, 927–941.

Mirmira, R. G., & Tager, H. S. (1989) *J. Biol. Chem. 264*, 6349–6354.

Muszkat, K. A., & Gilon, C. (1978) *Nature (London) 271*, 685–686.

Muszkat, K. A., Khait, I., & Weinstein, S. (1984) *Biochemistry 23*, 5–10.

Nakagawa, S. H., & Tager, H. S. (1986) *J. Biol. Chem. 261*, 7332–7341.

Nakagawa, S. H., & Tager, H. S. (1987) *J. Biol. Chem. 262*, 12054–12058.

Novotny, J., & Bruccoleri, R. E. (1987) *FEBS Lett. 211(2)*, 185–189.

Palmieri, R., Lee, R. W.-K., & Dunn, M. F. (1988) *Biochemistry 27*, 3387–3397.

Paselk, R. A., & Levy, D. (1974) *Biochim. Biophys. Acta 359*, 215–221.

Peking Insulin Structure Group (1971) *Peking Rev. 40*, 11–16.

Pocker, Y., & Biswas, B. B. (1980) *Biochemistry 19*, 5043–5049.

Pullen, R. A., Lindsay, D. G., Wood, S. P., Tickle, I. J., Blundell, T. L., Wollmer, A., Krail, A., Bradenburg, D., Zahn, H., Gliemann, J., & Gammeltoft, S. (1976) *Nature (London) 259*, 369–373.

Richards, T. M. (1975) *Annu. Rev. Biophys. Bioeng. 6*, 151–176.

Rupley, J. A., Renthal, R. D., & Praissman, M. (1976) *Biochim. Biophys. Acta 140*, 185.

Shih, H. H.-L., Brady, J., & Karplus, M. (1985) *Proc. Natl. Acad. Sci. U.S.A. 82*, 167–170.

Shoelson, S. E., Haneda, M., Blix, P., Nanjo, K., Sanke, T., Inouye, K., Steiner, D., Rubenstein, A., & Tager, H. (1983a) *Nature (London) 302*, 540–542.

Shoelson, S. E., Fickova, M., Haneda, M., Nahum, A., Musso, G., Kaiser, E. T., Rubenstein, A. H., & Tager, H. (1983b) *Proc. Natl. Acad. Sci. U.S.A. 80*, 7390–7394.

Smith, G. D., Swenson, D. C., Dodson, G. G., & Reynolds, C. D. (1984) *Proc. Natl. Acad. Sci. U.S.A. 81*, 7093–7097.
States, D. J., Haberkorn, R. A., & Ruben, D. J. (1982) *J. Magn. Reson. 48*, 286–292.
Steiner, D. F., Cunningham, D. D., Spigelman, L., & Aten, B. (1967) *Science 157*, 697–700.
Strickland, E. H., & Mercola, D. A. (1976) *Biochemistry 15*, 3875–3884.
Tager, H., Given, B., Baldwin, D., Mako, M., Markese, J., Rubenstein, A., Olefsky, J., Kobayashi, M., Kolterman, O., & Poucher, R. (1979) *Nature (London) 281*, 122–125.
Tager, H., Thomas, N., Assoian, R., Rubenstein, A., Saekow, M., Olefsky, J., & Kaiser, E. T. (1980) *Proc. Natl. Acad. Sci. U.S.A. 77*, 3181–3185.
Ullrich, A., Bell, J. R., Chen, E. Y., Herrera, R., Petrucelli, L. M., Dull, T. J., Gray, A., Coussens, L., Liao, Y. C., Tsubokawa, M., Mason, A., Seeburg, P. H., Grunfeld, C., Rosen, O. M., & Ramachandran, J. (1985) *Nature 313*, 756–761.
Weiss, M. A., Eliason, J. A., & States, D. J. (1984) *Proc. Natl. Acad. Sci. U.S.A.* 6019–6023.
Williamson, K. L., & Williams, R. J. P. (1979) *Biochemistry 18*, 5966–5972.
Wodak, S. J., Alard, P., Delhaise, P., & Renngboog, S. C. (1984) *J. Mol. Biol. 151*, 317–322.
Wollmer, A., Fleischhauer, J., Strassburger, W., Thiele, H., Bradenbury, D., Dodson, G., & Mercola, D. (1979) *Biophys. J. 20*, 233–243.
Wood, S. P., Blundell, T. L., Wollmer, A., Lazarus, N. R., & Neville, R. W. J. (1975) *Eur. J. Biochem. 55*, 531–542.
Wuthrich, K., Wider, G., Wagner, G., & Braun, W. (1983) *J. Magn. Reson. 155*, 311.

Effect of Monoclonal Antibody Binding on α–$\beta\gamma$ Subunit Interactions in the Rod Outer Segment G Protein, G_t[†]

Maria R. Mazzoni and Heidi E. Hamm*
Department of Physiology and Biophysics, University of Illinois, College of Medicine at Chicago, P.O. Box 6998, Chicago, Illinois 60680

Received May 1, 1989; Revised Manuscript Received July 31, 1989

ABSTRACT: The guanyl nucleotide binding regulatory protein of retinal rod outer segments, called G_t, that couples the photon receptor rhodopsin with the light-activated cGMP phosphodiesterase, can be resolved into two functional components, α_t and $\beta\gamma_t$. The effect of monoclonal antibody binding to the α_t subunit of G_t on subunit association has been investigated in the present study. It was previously shown that this monoclonal antibody, mAb 4A, blocks interactions with rhodopsin and its epitope was located within the region Arg^{310}–Phe^{350} at the COOH terminus of the α_t subunit. In this paper, we show that mAb 4A disrupts the G_t complex. G_t migrates in 5–20% linear sucrose density gradients as a monomer, with a sedimentation coefficient of 4.1 ± 0.07 S, while in the presence of mAb 4A, the α_t and $\beta\gamma_t$ subunits show sedimentation coefficients of 7.7 ± 0.2 and 3.7 ± 0.1 S, respectively. The $\beta\gamma_t$ subunit migrates with the same sedimentation rate as pure $\beta\gamma_t$. Nonimmune rabbit IgG does not modify the sedimentation behavior of G_t. The Fab fragment of mAb 4A also dissociates the G_t complex, as suggested by the change of the sedimentation rate of α_t. This effect of mAb 4A on G_t subunit association was also confirmed by immunoprecipitation studies in the presence of detergent. In the presence of detergent, subunit association is not affected, but the formation of G_t oligomers and, therefore, the nonspecific precipitation of $\beta\gamma_t$ subunit are reduced. An anti-peptide immune serum, raised against the last 10 amino acids from the carboxyl terminus of α_t, also immunoprecipitated the α_t subunit, and the $\beta\gamma_t$ subunit was found in the supernatant fraction. Monoclonal antibody 4A also blocks the pertussis toxin mediated ADP-ribosylation of α_t both in holo-G_t and in the purified α_t subunit. These results suggest either that the mAb 4A epitope is close enough to the site of $\beta\gamma_t$ interaction to dissociate binding or that antibody binding causes a conformational change on α_t causing loss of affinity for $\beta\gamma_t$.

A guanine nucleotide-binding regulatory protein, called transducin or G_t,[1] couples light-activated rhodopsin with the cGMP phosphodiesterase [for a review, see Stryer and Bourne (1986), Gilman (1987), Hurley (1987), and Liebman et al. (1987)]. Like all G proteins, G_t is a heterotrimer composed of two distinct subunits: α_t (39 kDa) and $\beta\gamma_t$ (β_t, 36 kDa; γ_t, 8 kDa). The α_t subunit binds GDP and GTP and in its GTP-bound form activates the cGMP phosphodiesterase. The activation is terminated when the bound GTP is hydrolyzed to GDP by an intrinsic GTPase activity (Wheeler & Bitensky, 1977). Although the $\beta\gamma_t$ subunit has not been shown to di-

[†]Supported by USPHS Grant EY-06062, NSF Grant DMB-8804861, and an unrestricted departmental grant from Research to Prevent Blindness. H.E.H. was the recipient of an NSF ROW Research Career Enhancement Award.
*To whom correspondence should be addressed.

[1] Abbreviations: G_t, photoreceptor guanyl nucleotide binding protein; α_t, α subunit of G_t; $\beta\gamma_t$, β and γ subunits of G_t; G_s and G_i, regulatory guanyl nucleotide binding proteins that mediate stimulation and inhibition of adenylate cyclase, respectively; G_k, guanyl nucleotide binding protein mediating muscarinic stimulation of cardiac potassium channels; G_o, guanyl nucleotide binding protein isolated from brain; mAb, monoclonal antibody; ROS, rod outer segment; BSA, bovine serum albumin; SDS, sodium dodecyl sulfate; GTPγS, guanosine 5′-*O*-(3-thiotriphosphate); MOPS, 3-(*N*-morpholino)propanesulfonic acid; DTT, dithiothreitol; PMSF, phenylmethanesulfonyl fluoride; PBS, phosphate-buffered saline; HEPES, 4-(2-hydroxyethyl)-1-piperazineethanesulfonic acid; CHAPS, 3-[(3-cholamidopropyl)dimethylammonio]-1-propanesulfonate; TCA, trichloroacetic acid.

0006-2960/89/0428-9873$01.50/0